Atomic and magnetic configurational energetics by the generalized perturbation method

Ruban, Andrei V.; Shallcross, Sam; Simak, S.I.; Skriver, Hans Lomholt

Published in:
Physical Review B Condensed Matter

Link to article, DOI:
10.1103/PhysRevB.70.125115

Publication date:
2004

Document Version
Publisher's PDF, also known as Version of record

Atomic and magnetic configurational energetics by the generalized perturbation method

A. V. Ruban
Applied Material Physics, Department of Materials Science and Engineering, Royal Institute of Technology, SE-100 44 Stockholm, Sweden

S. Shallcross
Department of Physics and Measurement Technology, University of Linköping, SE-581 83 Linköping, Sweden

S. I. Simak
Condensed Matter Theory Group, Physics Department, Uppsala University, Box-530, S-75121 Uppsala, Sweden

H. L. Skriver
Center for Atomic-scale Materials Physics and Physics Department, Technical University of Denmark, DK-2800 Lyngby, Denmark
(Received 3 May 2004; published 29 September 2004)

It is shown that, using the generalized perturbation method (GPM) with screened Coulomb interactions that ensures its consistency with the force theorem, one is able to obtain effective interactions that yield an accurate and physically transparent description of configurational energetics in the framework of the Korringa-Kohn-Rostoker method within the atomic sphere and coherent potential approximations. This is demonstrated with calculations of ordering energies, short-range order parameters, and transition temperatures in the CuZn, CuAu, CuPd, and PtCo systems. Furthermore, we show that the GPM can be used to obtain Heisenberg exchange interaction parameters, which, for instance, capture very well the magnetic configurational energy in bcc Fe.

DOI: 10.1103/PhysRevB.70.125115 PACS number(s): 71.15.−m, 71.23.−k, 61.66.Dk

I. INTRODUCTION

Many metallic alloys exhibit fascinating ordering behavior as a function of temperature and concentration,[1–3] and one of the important goals of alloy theory is therefore to be able to simulate these kinds of phenomena on the basis of first principles theory. Unfortunately, it is impossible, even with present day total-energy software, to calculate entirely from first principles the changes in the internal energy caused by changes of the atomic configurations in systems with several thousand atoms at the rate required by the statistical thermodynamics simulations. The time-honored solution to this problem, which we shall also use in the present paper, is to obtain the configurational energy needed in the simulations from an Ising-type Hamiltonian with so-called effective (cluster) interactions associated with specific changes in the local atomic configuration and obtained by first-principles total-energy calculations.

The most reliable way of obtaining effective interactions from first principles is thought to be the so-called Connolly-Williams or structure inverse method (SIM)[4,5] based on a mapping of the total energies (enthalpies of formation) of a number of predefined ordered structures onto an Ising-type configurational Hamiltonian. In principle, the accuracy of this approach is limited only by the accuracy of the total-energy calculations. However, it suffers from one problem: The range and the type, i.e., two-center, three-center, etc., of the effective interactions which should be included in the expansion of the configurational energy is not known *a priori*, and there is no systematic way of making the expansion converge. Furthermore, if the Hamiltonian or the expanded quantity are not well justified by the underlying physics, the structure inverse method may, in many practical applications, be rather cumbersome, even for ordinary homogeneous bulk systems such as Cu-Au and NiPt (see, for instance, Ref. 6). For inhomogeneous systems such as alloy surfaces or multicomponent alloys and alloys with magnetic degrees of freedom, it becomes highly impractical.[7] It has, however, been used in many studies of bulk binary alloys with great success.

The generalized perturbation method (GPM) suggested by Ducastelle and Gautier[1,8] offers an elegant and efficient alternative to the structure inverse method. The method is based on the coherent potential approximation (CPA) (Refs. 9–11) and originally formulated within tight-binding (TB) theory but later generalized in a straightforward manner[12–15] for the use in *ab initio* calculations based either on the Korringa-Kohn-Rostoker (KKR) method or the linear muffin-tin orbitals (LMTO) method in the atomic sphere approximation (ASA). Within the GPM the effective interactions can be derived with equal ease for both bulk and surface situations. Furthermore, the range and type of the interactions needed in the expansion of the configurational energy may easily be explored, allowing for a systematic convergence of the Ising-type Hamiltonian used in the thermodynamic simulations.

One important aspect of the application of the GPM is the way in which one accounts for the screened Coulomb interactions[1] that describe charge transfer effects. In the past these interactions have in many cases been neglected, leading to inaccurate effective interactions and a subsequent poor description of systems with a finite charge transfer. Hence, the effective interactions calculated by the GPM have in general been less accurate than those calculated for the same systems by the SIM. Recently, Ruban *et al.*[16,17] have developed a formalism that accounts for the screened Coulomb

interactions within the framework of the single-site approximation to density functional theory (DFT) and the force theorem,[18] and it was shown that the resulting screened (S)GPM interactions reproduce the configurational energetics for at least one system, namely a $Ni_{0.5}Pt_{0.5}$ alloy[17] with a high degree of accuracy.

The aim of this paper is twofold. First, we show that the success of the screened GPM interactions in describing the $Ni_{0.5}Pt_{0.5}$ alloy[17] is not fortuitous and that the screened GPM interactions lead to quantitative descriptions of the configurational energetics of a wide range of alloy systems. To do so, we consider the ordering energies, short-range order, and order-disorder transitions in fcc and bcc CuZn, CuAu, CuPd, and PtCo. We further demonstrate that magnetic exchange interactions calculated via the GPM can accurately reproduce the magnetic behavior of bcc Fe. Second, we wish to emphasize that through the GPM one may obtain a very clear picture of the physics behind ordering in these systems. It will be shown that Fermi surface effects, volume dependence of the electron density, and band-filling mechanisms may be distinguished clearly in the GPM.

The layout of the paper is as follows. In Sec. II we define the effective interactions that are used and describe the GPM that we advocate for finding them. Details of the calculational methods will be presented in Sec. III. The remainder of the paper will then describe our calculations of fcc CuZn, bcc CuZn, CuAu, CuPd, PtCo, and fcc and bcc Fe, presented in Secs. IV–IX, respectively. In Sec. X we conclude.

II. METHODOLOGY

A. Effective cluster interactions

In configurational thermodynamics the underlying crystal lattice is usually taken to be topologically fixed, so that the possibility of defect formation is excluded. In this case the distribution of atoms on the lattice is given by occupation numbers, c_i, or equivalently spin-like variables, $\sigma_i=2c_i-1$, which take on values 1 and 0, or 1 and -1, respectively, depending on whether there is an atom A or B at site i in the case of a binary A_cB_{1-c} alloy. In multicomponent systems there should be an additional index running through all alloy components but one. The alloy configuration can then be uniquely determined by a set of correlation functions for clusters of order n (which consist of n sites) and type s (labeling its geometric class)

$$\tilde{\xi}_s^{(n)} = \frac{1}{n}\sum_{p\in s}\prod_{i=1,n}\sigma_{i_p}, \tag{1}$$

where the summation runs over all the clusters in the system.

As has been shown,[19] they form in general a complete basis for expanding any thermodynamic property as a function of alloy configuration if the range of interactions is finite. In particular, the configurational energy is

$$E_{conf} = \sum_{n,s}\tilde{V}_s^{(n)}\tilde{\xi}_s^{(n)}, \tag{2}$$

where $\tilde{V}_s^{(n)}$ is the effective cluster interaction (ECI) that corresponds to the cluster of order n and type s. The same form of the configurational energy can, of course, be obtained phenomenologically. In this way one starts from the interatomic potentials, $v_{AB\ldots B}^{(n)} \equiv v^{(n)}(\sigma_i,\sigma_j,\ldots,\sigma_k)$, which are the interaction energies of the group of $A,B,\ldots,B$ atoms in the corresponding positions of the cluster

$$\tilde{V}_s^{(n)} = \frac{1}{2^n}\sum_{\sigma_1,\sigma_2,\ldots\sigma_n=1,-1} v^{(n)}(\{\sigma_1,\sigma_2\ldots,\sigma_n\})\prod_{i=1,n}\sigma_i = \frac{1}{2^n}V_s^{(n)}. \tag{3}$$

Here, we have defined concentration-variable effective interactions $V_s^{(n)}$ which are usually used in GPM applications and which appear in the configurational Hamiltonian (2) if instead of spin-variables, σ_i, the occupation numbers c_i are used. In the following all the results and formulas are given using this latter notation.

An important point is that the ECI in Eq. (2) will in general depend on parameters such as concentration and volume. However, the very complex energy space $E(\{\mathbf{R}_i\},\{c_i\},V)$ may be mapped onto a Hamiltonian that is independent of these parameters. In fact, this is usually the case in the SIM simply out of necessity, there being for a reasonable size of the supercell too few structures that may be generated at a fixed concentration. For ECIs that are either strongly volume-or concentration dependent, their mapping onto a Hamiltonian independent of them will naturally lead to interactions of a highly multisite and long-range character. This may be further exacerbated if relaxed geometries are used for the input structures. However, such interactions have no physical basis.

This can be illustrated with two examples. First, it is known that a large part of the volume dependence of the total energy in metals, especially nontransition metals, can be related to the average electron density in the interstitial region (see, for instance, Refs. 20 and 21). This of course has no connection to interatomic interactions at all. However, one could map this dependence onto some volume-independent fitting ECIs, which must then become highly multisite in character to mimic the formation of the corresponding average density of some region with different amounts of A and B atoms. On the other hand, the ECI may display some marked concentration dependence. This can arise from features of the underlying electronic structure of the alloy, for example band filling with concentration. Again, it is of course feasible to map these ECIs onto concentration-independent fitting ECIs. These, though, will contain higher order terms not present in the concentration-dependent interactions.[22,23] In general, the order of the resulting ECI will be $n+k$, where n is the order of the concentration-dependent ECI and k is the order of the polynomial which describes its variation with concentration.

In both cases it is obvious that although ECIs may be determined that are independent of important parameters, a great deal of the underlying physics may be obscured. In what follows we will give examples of both cases: the fcc CuZn system, which shows a dramatic dependence on concentration, and the CuAu system, which shows almost no concentration dependence but a strong volume dependence coming from the large size mismatch in this system.

B. Generalized perturbation method

Here, we briefly show how the GPM effective interactions may be derived. The presentation is along the lines usually found in the literature, and for a thorough derivation of the GPM in the KKR-CPA formalism we recommend Refs. 12 and 24. As a starting point, one may note that a single specific ECI may, in fact, be obtained directly from first-principles calculations. One has to prepare two systems having exactly the same correlation functions of all the types corresponding to the non-negligible effective interactions except the one of interest, and then obtain their total energies (see, for instance, Ref. 17). The ECI is then simply the difference in the total energies properly normalized. The main problem with the practical implementation of this scheme is that it requires the use of very large supercells, even when only pairwise interactions for the nearest-neighbor shells are required. It is also obvious that it is difficult to use this scheme in a perturbative way, since going from one system to the other in general requires a rearrangement of most of the atoms on the underlying lattice.

A simple way to avoid these problems is the introduction of an effective medium which represents a random alloy configuration on average, and then to consider the energetics of the corresponding clusters embedded in this effective medium. In the simplest case, and that used in the GPM, the effective medium represents a homogeneous random alloy without any short-range order on the underlying lattice whose correlation functions satisfy the following condition: $\xi_s^{(n)}=(\xi^{(1)})^n=\langle\sigma\rangle^n$. This of course cannot be done exactly, and the latter is achieved, for instance, by the use of the CPA.

Once the effective medium is determined, ECIs can be found using definition (3). The spin product in (3) takes on values 1 and −1 depending on whether the number of A atoms is even or odd in the cluster $\{\sigma_1,\sigma_2,\ldots,\sigma_k\}$. In other words the effective interaction is the difference of the total energies of two systems: one which consists of all the clusters with an even number of A atoms embedded in the effective medium of the random alloy and another with exactly the same set of clusters but with an odd number of A atoms (interactions between clusters being excluded)

$$V_s^{(n)}=E_{A-even}-E_{A-odd}. \tag{4}$$

Important here is the fact that the set of A-odd clusters can be obtained from the set of A-even clusters simply by choosing a fixed site in each cluster and then making an exchange of A and B atoms between all the different pairs of A-even clusters. Besides, it also can be shown (as a consequence of the orthogonality of the cluster correlation functions) that in this case all contributions from the interactions of lesser order will be canceled, and thus $V_s^{(n)}$ represents a genuine n-site interaction.

The difference in total energies of the two sets of clusters in (4) can be obtained with the use of the force theorem,[18] according to which the change in energy from embedding the clusters is given by the change in the one-electron energy and the change in the electrostatic interaction due to the perturbation. The one-electron energy term can be derived in an explicit form through Lloyd's formula in the Green's function formalism which determines the change in the integrated density of states of a reference system due to the embedding in this system of some particular cluster. As has been shown by Gonis,[12,25] this is then given by the following expression:

$$V_s^{(n)\text{-}one\text{-}el}=-\frac{1}{\pi}\,\mathrm{Im}\int^{E_F}\mathrm{Tr}\ln\left[\prod_{p\in A\text{-}even}Q_p\left(\prod_{p\in A\text{-}odd}Q_p\right)^{-1}\right]. \tag{5}$$

Here, Q_p are the cluster matrices defined as

$$Q_{ij}=\delta_{ij}-t_i\tilde{g}_{ij}(1-\delta_{ij}), \tag{6}$$

in terms of the single-site scattering matrix, t_i, for site i and the path operator $\tilde{g}_{ij}$ of the reference system yielding the scattering between the ith and jth sites in the cluster. δ_{ij} is the Kronecker delta symbol. The integration over energy in (5) is up to the Fermi energy of the reference system. As has been mentioned, the reference system is a random alloy, which is homogeneous for ordinary Bravais lattices in the sense that the single-site scattering matrix of the alloy components is the same independently of their local environment in the cluster. That is

$$t_i=[1+(\tilde{P}-P_i)\tilde{g}_0]^{-1}(\tilde{P}-P_i), \tag{7}$$

where the LMTO (KKR-ASA) potential function, P_i, takes on values P^A or P^B if site i is occupied by either an A or B alloy component, and $\tilde{g}_0$ is the on-site CPA scattering path operator, and therefore t_i also takes on values t^A and t^B depending on the type of atom. The coherent potential function, $\tilde{P}$, represents the CPA effective medium which yields the electronic structure of the random A_cB_{1-c} alloy and satisfies the CPA self-consistency equation

$$ct^A+(1-c)t^B=0. \tag{8}$$

The GPM effective interactions now can be obtained by expanding the logarithm and leaving in the expansion only those terms which correspond to the lowest order of scattering on the whole cluster. That is

$$V_s^{(n)-GPM}=-\frac{1}{\pi}\,\mathrm{Im}\int^{E_F}\sum_{p\in s}\mathrm{Tr}(\Delta t_i\tilde{g}_{ij}\Delta t_j\cdots\Delta t_k\tilde{g}_{ki})_s, \tag{9}$$

where $\Delta t_i=t^A-t^B$ and the summation is performed over all irreducible paths starting and ending on the same site and going only once through each site. In the case of pair and three-site interactions there is only one irreducible path, but in general $(n-1)!/2$ such paths must be taken into consideration.

The higher order scattering contributions can be partly accounted for by the expression[24]

$$V_s^{(n)-GPM}=-\frac{1}{\pi}\,\mathrm{Im}\int^{E_F}\sum_{p\in s}\mathrm{Tr}\ln[1-(\Delta t_i\tilde{g}_{ij}\Delta t_j\cdots\Delta t_k\tilde{g}_{ki})_s]. \tag{10}$$

In the limit $c\to 0(1)$ this expression yields "renormalized" effective interactions (see Ref. 12) given by (5). However,

one should be careful using (10) in the whole concentration range, since close to $c=0.5$ it usually overestimates the multisite contribution. At this concentration, for instance, the contribution from the doubly repeated scattering process on couples of atoms, which gives a four-site contribution to the renormalized effective pair interactions is proportional to $(1-2c)$,[12] and thus is equal to zero. However, according to (10) such a term does not vanish and is, in fact, clearly the leading term in the multiatom scattering. Nevertheless, the difference between (9) and (10) is an important quantity since it gives an indication of the importance of multisite interactions for a given cluster.

C. Screened electrostatic interactions

It now remains to derive the screened Coulomb contribution to the GPM interactions. Such a derivation has already been given by Ducastelle[1] in the framework of the Hartree-Fock and tight-binding approximations, but here it should be established in a manner consistent with (1) the force theorem[18] and (2) the electrostatics in the single-site DFT-CPA formalism[16] used to obtain the one-electron contribution (9).

As shown in Refs. 16 and 17, the electrostatic energy of a random alloy may be given by screened Coulomb interactions. In general these appear due to nonzero net charges on the atomic spheres that artificially divide the crystal space. On the other hand, the CPA effective medium is electroneutral and this means that every charged atomic sphere must have associated with it a screening charge. This screening charge provides the necessary neutrality condition for solving Poisson's equation for every atomic sphere in the single-site DFT-CPA, and leads to the on-site screened Coulomb interaction,[16,17] which for every site is given by

$$\epsilon_i = -\frac{e^2}{2}\frac{\alpha_{scr}}{S}q_i^2 = \frac{e^2}{2}q_i\int_S^\infty d^3r\frac{\rho_{scr}^i(\mathbf{r})}{r}, \tag{11}$$

where q_i is the net charge inside atomic sphere $i=A$ or $i=B$, $\rho_{scr}(\mathbf{r})$ the density screening the net charge, and S the atomic sphere radius which for simplicity is taken to be the same for the two alloy components and equal to the average Wigner-Seitz radius.

The electroneutrality of the effective medium also means that in the exchange of A and B atoms which takes place when calculating the pairwise GPM interactions one should exchange the atomic spheres together with their corresponding screening densities. This is shown schematically in Fig. 1. Only in this way may the electroneutrality condition in the force theorem be satisfied.

The change in the electrostatic energy of the two systems is an *intersite* screened Coulomb interaction. It can be obtained as the difference upon exchange of the electrostatic energy projected onto sites **0**. One should include only the interaction of the net charge at site **0** with the net charge at site **R** and *its screening* charge. The resulting contribution to the pair effective interaction from the screened Coulomb interactions is

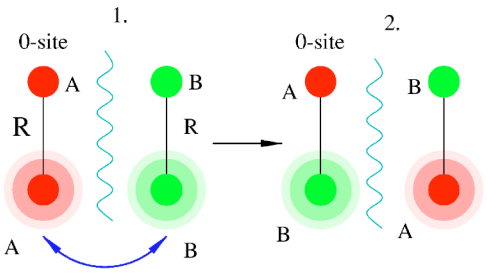

FIG. 1. (Color online). A schematic definition: Two systems, whose energy difference yields effective pair interactions at distance R.

$$V_{scr}^{(2)}(R) = \frac{e^2}{2}\left\{q_A\left(\frac{q_A-q_B}{R}-\int_S^\infty d^3r\frac{\rho_{scr}^A(\mathbf{r})-\rho_{scr}^B(\mathbf{r})}{|\mathbf{r}-\mathbf{R}|}\right)\right.$$
$$\left.+\,q_B\left(\frac{q_B-q_A}{R}-\int_S^\infty d^3r\frac{\rho_{scr}^B(\mathbf{r})-\rho_{scr}^A(\mathbf{r})}{|\mathbf{r}-\mathbf{R}|}\right)\right\}$$
$$=\frac{e^2}{2}(q_A-q_B)^2\frac{\alpha_{scr}(R)}{S}. \tag{12}$$

Here, $\alpha_{scr}(R)$ is the intersite screening constant.

In general the intersite screening constant is found to vary from system to system and to exhibit concentration and volume dependence, although the latter is often very weak. It may be obtained in supercell calculations as described in Refs. 16 and 17. Such calculations are, in fact, quite time consuming even using an order-N method such as the locally self-consistent Green's function technique,[26,27] since the supercell must be large enough to exclude any overlap of the screening densities leading to supercells containing several hundred atoms for simple Bravais lattices. At the moment such calculations also include errors due to the use of the atomic sphere approximation, albeit with multipole moment corrections for the charge density.

To summarize, the screened GPM (SGPM) interactions include both a one-electron term, $V^{GPM}(\mathbf{R})$ given by (9), and a pairwise screened Coulomb interaction $V_{scr}^{(2)}(\mathbf{R})$ given by (12)

$$V^{(2)}(\mathbf{R}) = V^{(2)-GPM}(\mathbf{R}) + V_{scr}^{(2)}(\mathbf{R}). \tag{13}$$

The SGPM interactions defined above clearly involve a number of approximations, and one may worry about the accuracy with which they will represent the true configurational energy in actual thermodynamic simulations. The first approximation is of course the use of the single-site CPA, the error of which cannot in general be specified. Furthermore, since the SGPM interactions are calculated by perturbation theory from the CPA *random* alloy reference system they will not only depend on concentration and volume but will also, in general, be *configuration* dependent, for example in inhomogeneous systems. One may therefore fear that such interactions will not reproduce the energies of *ordered* alloys with the necessary accuracy. However, below we shall show that the SGPM interactions lead to ordering energies of a

wide spectrum of structures which agree with the values from direct DFT calculations. For low-symmetry structures which possess considerable and specific polarization effects the SGPM will in general introduce errors. However, these structures usually have high energies and their weight in statistical thermodynamics simulations is very low.

D. Local relaxation interactions

It is a fundamental problem in the present approach as well as in the SIM that the effective interactions are calculated for a fixed underlying lattice and, as a result, lattice strain effects are neglected. These effects will be especially important in systems with a large size mismatch and must be included for quantitative predictions. The strain effects may manifest themselves either as long-range interactions causing a symmetry lowering global distortion of the lattice, or as symmetry preserving local relaxations. We remedy this latter case by introducing a specific term H_{rel} in the Hamiltonian to treat local relaxations in the effective tetrahedron model (ETM)[28]

$$H_{rel} = \tfrac{1}{4} \sum_{i,j,k,l} V_{rel}(\sigma_i, \sigma_i, \sigma_i, \sigma_i), \tag{14}$$

where σ_i are the spin variables for the corresponding tetrahedron vertices i, j, k, l and the summation is performed over all the tetrahedra of the nearest neighbors in the alloy. It was shown in Ref. 28 that the relaxation energies produced by this approximation are in rather good agreement with direct calculation, at least for the late transition and noble metals. As was further shown in Ref. 28 this Hamiltonian may be transformed into terms of pair, triangle, and four-site Ising-type interactions.

III. CALCULATIONAL DETAILS

The electronic structure, total energies and other properties of random and ordered alloys have been obtained in Korringa-Kohn-Rostoker (KKR) self-consistent density functional calculations in the atomic sphere approximation (ASA).[29] The results include the muffin-tin correction to the Madelung energy,[30] needed to obtain an accurate description of ground-state properties in the ASA, and the multipole moment correction to the Madelung potential and energy[29] (+M) which significantly improves the accuracy of, in particular, the ordering energies by taking into account the nonspherical parts of the charge polarizations.

Although the self-consistent calculations have been performed within the local density approximation (LDA) with the Perdew and Wang parametrization of the exchange-correlation potential,[31] the total energies have been obtained in three different approximations for the exchange-correlation energy: the LDA,[31] local Airy gas (LAG),[32] and generalized gradient approximation (GGA).[33] The partial waves in the KKR-ASA calculations have been expanded up to $l_{max}=3$ inside atomic spheres, while the multipole moments of the electron density have been determined up to $l^M_{max}=6$ for the multipole moment correction to the Madelung energy. The core states have been recalculated after each iteration. The number of k points in the integration over the Brillouin zone, performed by means of the Monkhorst-Pack scheme,[34] varied depending on the system and type of calculations. For instance, due to the long-range character of the effective interactions in $Cu_{0.75}Pd_{0.25}$ we used 8240 k points in the irreducible wedge of the Brillouin zone of the fcc lattice. A large number of k points was also used in the calculations of the long-period superstructures (LPS) in Cu_3Au and Cu_3Pd, varying from 1300 to 2128 points in the irreducible wedge of the body-centered tetragonal Brillouin zone for the LPS5 and DO_{22} structures, respectively.

The electronic structure and ground-state properties of the random alloys have been obtained in the DFT single-site KKR-ASA-CPA calculations with the Coulomb screening potential, V^i_{scr}, and energy E_{scr}[17] defined as

$$V^i_{scr} = \frac{\delta \epsilon_i}{\delta \rho_i} = e^2 \alpha_{scr} \frac{q_i}{S}, \tag{15}$$

$$E_{scr} = -\beta_{scr} \sum_i c_i \epsilon_i,$$

where c_i is the concentration of the ith alloy component and ϵ_i is given by (11). Here, we have also introduced an additional screening constant, β_{scr}, describing the multipole-multipole Coulomb interactions.[17] The two screening constants have been obtained in "impurity"-like calculations described in Refs. 16 and 17 using the locally self-consistent Green's function (LSGF) method.[26,27]

The full potential Vienna *ab initio* simulation package (VASP)[35,36] was used in the direct first-principles calculations of the local lattice relaxations in bcc random $Cu_{0.5}Zn_{0.5}$ alloys modeled by special quasirandom structures as well as in the ordering energy calculations in the fcc $Cu_{0.75}Zn_{0.25}$ and bcc $Cu_{0.5}Zn_{0.5}$ alloys. These calculations made use of the projector augmented wave (PAW) method[37] as implemented in the VASP and described in detail in Ref. 38 that has been shown in many studies to have the same accuracy as all-electron full potential methods. In the calculations the energy cutoff was set to 276.7 eV. Exchange and correlation effects in both systems were treated in the framework of the generalized gradient approximation of Perdew and co-workers,[33] usually referred to as PW91. The integration over the Brillouin zone was done on special k points determined according to the Monkhorst-Pack scheme.[34] All necessary convergence tests in the VASP calculations were performed, and generally the required total energy convergence (within 0.2 mRy/atom) was reached for 18 to 455 k points in the irreducible wedge of the Brillouin zone depending on the structure and total number of atoms.

IV. FCC CUZN ALLOYS (α-BRASS)

CuZn is a classic Hume-Rothery system where one can find the whole range of usual metallic structures from fcc Cu to hcp Zn through the bcc high-temperature random alloys. CuZn alloys form the simplest B2 ordered structure and at the same time a quite complicated Cu_5Zn_7 ordered phase (γ-brass). The stability of the different phases of CuZn can

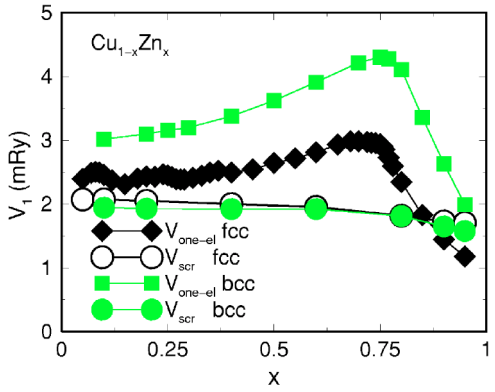

FIG. 2. (Color online) The one electron and screened Coulomb contributions to the nearest-neighbor interaction in fcc and bcc $Cu_{1-x}Zn_x$ as a function of Zn concentration, x, at a fixed Wigner-Seitz radius, $S=2.735$ a.u.

be accounted for by the presence of the specific features in the electron density of states which appear due to the scattering of free-electron-like s states on the corresponding Bragg planes[39–41] (the d states, being almost full, do not participate in the bonding).

Since the bonding is dominated by s states, local environment effects in the one-electron spectrum should be very small. Further, the small size mismatch between Cu and Zn means that phase stability is not determined to any large extent by lattice relaxation effects. These features make CuZn a very attractive system for deploying CPA and GPM calculations,[26,42–46] and in fact it was one of the first systems where such an approach was used to calculate the phase diagram (on the fcc and bcc lattices) from first principles.[47] These calculations were performed without the contribution from the screened Coulomb interactions. However, the effective charge transfer, defined as the difference in the net charges of the alloy components in a CPA calculation, is about 0.2 e in α-brass. This is not small and indicates that electrostatic effects cannot be neglected. It follows that calculations of the ordering energies and short-range order parameters in this system may serve as a useful test of the SGPM formalism.

A. Effective interactions

We start with some general observations concerning the effective interactions in the CuZn system. Figure 2 shows the concentration dependence of the one-electron and Coulomb parts of the SGPM interactions for the first coordinate shell. One notes that these two terms are of similar magnitude, and so one cannot neglect the screened Coulomb interactions in this system. In these calculations the lattice spacing has been kept fixed and therefore what is seen here results exclusively from the band filling as the concentration of Zn, which has one more electron than Cu, is increased. The dramatic change in the strength of the GPM interactions occurs at about 75% concentration of Zn in both the fcc and bcc Cu–Zn alloys. As one can see in Fig. 3, the Fermi energy at this concentration appears to be in the pseudogap separating bonding and antibonding states. This is due to Bragg-type

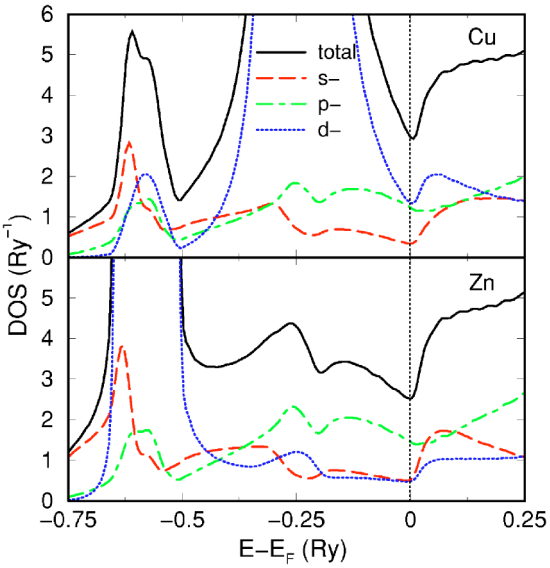

FIG. 3. (Color online) Partial and local density of state of the bcc $Cu_{25}Zn_{75}$.

reflections of the s electrons from the fcc (111) and bcc (110) planes.[40] With increasing Zn concentration the antibonding states become occupied, which leads to the dramatic drop in the GPM interactions. In general such changes in the occupation of bands may have a strong influence on the thermodynamic properties of alloys, for instance the Debye temperature and shear moduli in AgZn (isoelectronic to CuZn) show such a behavior.[48]

The complex behavior of the interactions seen in this fixed volume study will obviously carry over to the case where the volume is allowed to change with concentration. Thus, the construction of an Ising-type Hamiltonian with concentration-independent n-site interactions such as is used in the SIM for the *whole* concentration range will necessarily involve n values so high that the convergence of the expansion is difficult to control. This may be the reason why Muller *et al.*[49] restrict their SIM study of this system to the Cu-rich alloys, which excludes the sudden drop in the effective interactions at high Zn concentrations. In the SGPM, with its concentration-dependent interactions however, the contribution from multisite interactions is very small and can be neglected.[50]

B. Long-range order: Ordering energies

It is useful to test the quality of the SGPM interactions by comparing ordering energies calculated directly from first principles with those obtained by the SGPM according to the expression

$$E_{ord}^{\gamma} = \tfrac{1}{2}c(1-c)\sum_i z_i \alpha_i^{\gamma} V_i^{(2)}, \tag{16}$$

where α_i^{γ} are the Warren-Cowley short-range order parameters of the corresponding γ structure and z_i the coordination number for the ith coordination shell of the fcc lattice.

In Fig. 4 we make this comparison for the $L1_2$, DO_{22}, and DO_{23}–Cu_3Zn structures calculated at a fixed lattice spacing.

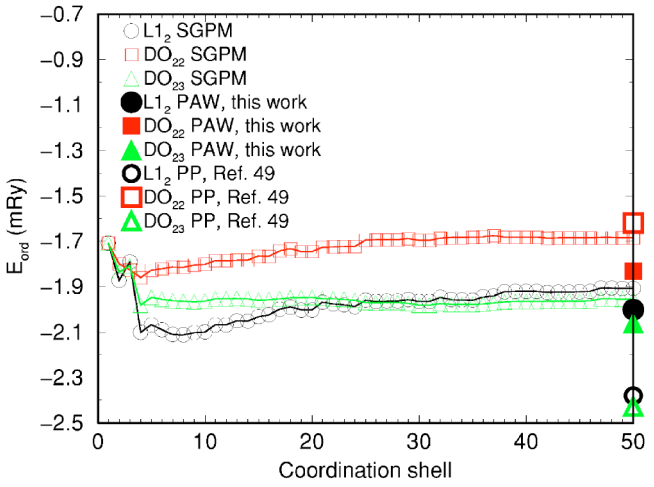

FIG. 4. (Color online) The ordering energies of $L1_2$, DO_{22}, and DO_{23} Cu_3Zn phases obtained from the SGPM interactions and in the direct FP-PAW calculations at $a=3.7$ Å. We also show the pseudopotential results by Muller *et al.* (Ref. 49.

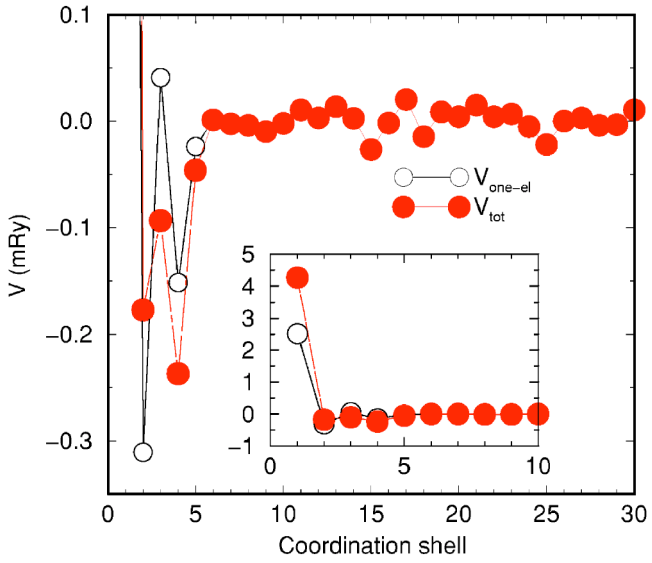

FIG. 5. (Color online) Pair SGPM interactions in fcc random $Cu_{0.69}Zn_{0.31}$ alloy at $a=3.688$ Å.

The agreement between the first-principles VASP-PAW energies and those from the SGPM is clearly excellent as is the agreement with the ordering energies obtained in our direct KKR-ASA(+M) calculations (not shown). However, there is an unexpected disagreement between our VASP-PAW results and those obtained in the pseudopotential calculations by Muller *et al.*[49] Although the ordering energies in the latter case have been obtained at theoretical equilibrium volumes and geometries different from ours, we believe that the disagreement is too large to be accounted for by volume and geometry effects, as the ordered structures are very similar and the size mismatch of Cu and Zn is small.

Also shown in Fig. 4 is the behavior of the ordering energies in Cu_3Zn as functions of the cutoff in the summation over coordinate shells in (16). It is seen that the stability of the DO_{23} phase is determined by the long-range *tail* of the pair interactions. In fact, the DO_{23} phase does not become stable until after the 25th coordination shell, which is to be expected in a system dominated by free-electron-like *s* states.

In view of the slow convergence exhibited by the ordering energies in Cu_3Zn, one must conclude that the cutoff at 15 shells used in the SIM calculations of Ref. 49 does not lead to interactions that are useful fitting parameters as they cannot reflect the physics behind the stability of the DO_{23} phase. This clearly highlights one of the problems of the SIM: In practice it is almost impossible to perform systematic convergence tests of the interaction range, because to establish the long-range behavior by the SIM requires very large basis structures that do not lend themselves easily to first-principles calculations.

C. Short-range order: Comparison with experiment

The ordering in α-brass has been thoroughly investigated experimentally by the diffuse neutron scattering technique.[51,52] In particular, the short-range order parameters have been determined for a $Cu_{0.69}Zn_{0.31}$ alloy at 473 K, providing the opportunity to test the quality of the SGPM interactions through a comparison of the calculated and measured short-range order parameters.

To make a meaningful comparison between theory and experiment, one must first determine the lattice parameter which is to be used in the calculations of the SGPM interactions. This is an important issue because neither the effective interactions nor the ordering energies are variational with respect to changes in the lattice parameter. In fact, although the effective interactions are much less sensitive to the different approximations for exchange and correlation than ground-state properties, they do in general show a strong dependence on the interatomic distances. It follows that the SGPM interactions to be used in the Monte Carlo simulations of the short-range order parameters in α-brass should be determined at a lattice spacing corresponding to the temperature used in the experimental situation rather than 0 K.

To this end we first find the theoretical equilibrium lattice constant of $Cu_{0.69}Zn_{0.31}$ by KKR-ASA(+M)-CPA calculations using the electrostatic screening constants $\alpha_{scr}=0.56$ and $\beta_{scr}=0.92$ (see Sec. II C) and the GGA for the exchange-correlation energy. This yields zero- and room-temperature lattice constants equal to 3.674 Å 3.694 Å, respectively. The latter has been calculated in the Debye-Grünesen model,[53,54] and is in reasonable agreement with the experimental room temperature value of about 3.688 Å.[55] The Debye-Grüneisen model further allows us to estimate the lattice spacing of the $Cu_{0.69}Zn_{0.31}$ alloy at 473 K, which we find to be equal to 3.705 Å. We consider this to be best estimate of the relevant experimental lattice spacing which we therefore use in the subsequent KRR-ASA-CPA calculations of the SGPM effective interactions.

The SGPM interactions calculated for a random α-$Cu_{0.69}Zn_{0.31}$ alloy are presented in Fig. 5. It is seen that the nearest-neighbor interaction is dominating in this system, followed by those of the 2nd, 3rd, and 4th coordination shells which are one order of magnitude smaller. All other interactions are two or more orders of magnitudes below the

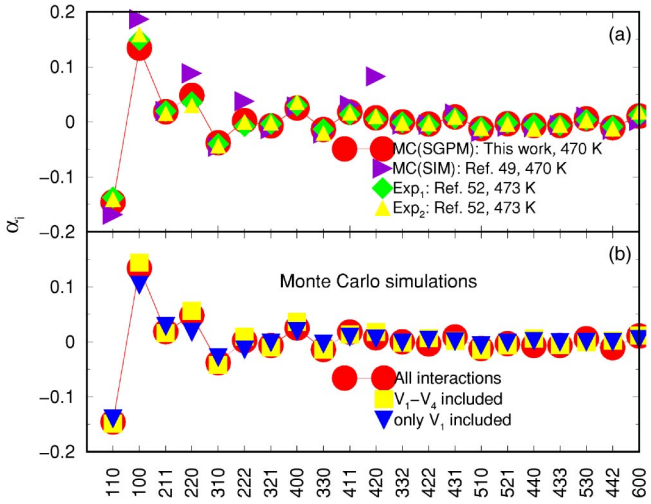

FIG. 6. (Color online) (a) The calculated and measured Warren-Cowley SRO parameters in fcc $Cu_{69}Zn_{31}$. (b) MC simulations (T =470 K) with restricted set of pair interactions.

dominant nearest-neighbor interaction but, as we have seen in Fig. 4, it is in fact the contribution from these minute terms which in the end favors the DO_{23} type of ordering over the $L1_2$.

To provide a quantitative analysis of short-range order in random alloys one must account for the local relaxations effects. This we do in the ETM, Sect. II C, and therefore the complete Hamiltonian to be used in the Monte Carlo simulations for random $Cu_{0.69}Zn_{0.31}$ at 473 K include the interactions shown in Fig. 5 plus the relaxation term in Eq. (14). In this case the ETM yields a relaxation energy of −0.3 mRy.

In the top panel of Fig. 6 we compare the Warren-Cowley SRO parameters obtained by the complete Hamiltonian described above with the experimental data.[51,52] The agreement between the present simulations and the experiments is seen to be excellent for all coordination shells. Also displayed are the results of Muller and Zunger[49] obtained by Monte Carlo simulations based on the mixed-space cluster expansion (MSCE) Hamiltonian with effective interactions obtained using the structure inverse method. In this case the simulations agree less well with experiment for shells number 2, 4, 6, and 11. It is difficult to speculate as to the origin of these deviations, but we suspect that it may partly be caused by problems with the total energy calculations, cf. the ordering energies in Fig. 4. It is clear, however, that the SIM effective interactions should be quite different from the fully converged interactions, since the longe-range tail of the pair interactions, which leads to the stabilization of the DO_{23} structure, is renormalized among the others.

The remarkable agreement between the calculations by the SGPM and the experimental results for the SRO, on one hand, and the fact that the interaction at the first coordination shell strongly dominates all the others, on the other, poses a question concerning the role of the more distant interactions in the formation of the SRO at high temperature. To make this point more clear, we estimate the strength of the interaction V_i by the measure $\nu_i = 1/2 V_i z_i$, where z_i is the coordination number. We find for the first four interactions: $\nu_{110,100,211,220} = 1014$, −24, −43, −56 K, and for the next 5: $\nu_{310,222,321,400,330} = -21$, 0.1, −2.4, −0.5, −4.5 K. That is, the interactions beyond the first coordination shell are at least two orders of magnitude smaller than that at the first coordination shell, ν_{110}, and one order of magnitude smaller than the 450 K at which the experiments and the simulations are carried out. In spite of this, one can clearly see relatively strong oscillations in the SRO parameters at the ninth coordination shells mentioned above.

To find the main source of the oscillatory behavior in the SRO parameters we have performed MC simulations for the same 21 coordination shells used in the complete calculation, but included only either the first or the first four pair interactions included in the simulations. The results are presented in the lower panel of Fig. 6. It is truly curious to observe that the single interaction at the first coordination shell reproduces the oscillatory behavior of the SRO parameters up to the ninth coordination shell. This means that the observed values of the SRO parameters for these coordination shells are mainly determined by the nearest-neighbor interaction. In other words, the SRO parameters at the first nine coordination shells in α-brass are to a large degree induced by nearest-neighbor interactions through higher order correlation effects, and their value and sign are determined by the geometry of the fcc lattice.

V. ORDER-DISORDER TRANSITION IN β-BRASS

The order-disorder transition in bcc CuZn alloys is an extensively studied second-order phase transitions used as a model system in the first fundamental experimental work on critical scattering by Als-Nielsen and Dietrich.[56,57] The transition occurs at about 740 K on the Cu-rich side of the equiatomic composition. The ordered low-temperature phase has the quite simple B2(CsCl) structure which, however, is not the ground-state structure of stoichiometric $Cu_{0.5}Zn_{0.5}$. The latter forms γ-brass, which according to Paxton[40] may be related to the appearance of additional Bragg planes that lower the one-electron energy.

The transition in β-brass has already been calculated by Turchi *et al.*[47] using the cluster variation method with GPM interactions, and these authors found a critical temperature of 730 K which is in very good agreement with experimental data. The agreement, however, must be accidental since their interactions do not include the (screened) Coulomb interactions which are quite large in this system, at least for the first coordination shell, as can be seen in Fig. 2.

Here, we use the SGPM interactions to simulate the order-disorder phase transition in CuZn on a bcc lattice. As in the previous section we include the relaxation term (14) and calculate the interactions at the lattice parameter relevant to the high-temperature experimental situation. In this case we use a value of 2.987 Å as estimated by the Debye-Grüneisen model at 800 K.

To judge the validity of the SGPM interactions, we compare in Fig. 7 the ordering energies calculated by (16) with those obtained in the direct VASP total-energy calculations. It is clearly seen that the SGPM interactions yield a quantitatively accurate description of the ordering in β-brass. The largest discrepancies between the direct calculations and the

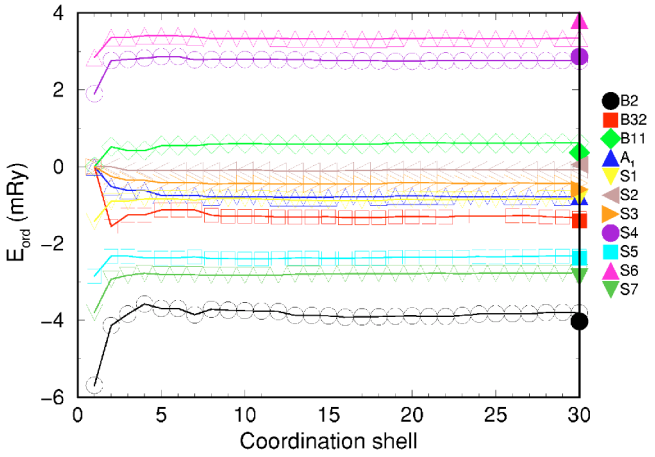

FIG. 7. (Color online) The ordering energies of 11 different ordered equiatomic CuZn alloys (including 7 generated specifically for configurational energy test: S1–S7) obtained from the SGPM interactions and in the direct FP-PAW calculations.

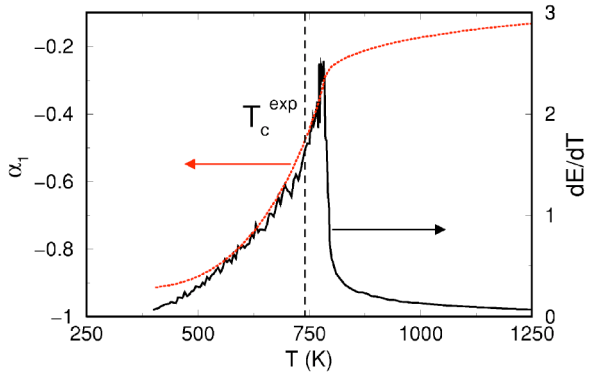

FIG. 8. (Color online) The calculated specific heat and Warren-Cowley SRO parameter at the first coordination shell in $Cu_{0.52}Zn_{0.48}$ obtained in the Monte Carlo simulations.

SGPM results are found in the "phase-separated"-like structures which have positive ordering energies. However, as these structures represent configurational states, the statistical weights of which will be almost zero, the corresponding errors will be of little consequence in the thermodynamic simulations.

To include the local lattice relaxation energy in the Hamiltonian for the Monte Carlo simulations the effective tetrahedron model[28] is modified to accommodate the bcc lattice.[58] Thus, the relaxation energy has the same form as for the fcc lattice (14), the only difference being that the relaxation interactions are determined for the smallest tetrahedron on the bcc lattice, which is the tetrahedron formed by 4 sides connecting the nearest-neighbor sites and 2 sides connecting the nearest-neighbor sides. The relaxation interactions have been calculated in the GGA and yield a relaxation energy of a random $Cu_{0.5}Zn_{0.5}$ alloy of −0.55 mRy, which compares well with the values of −1.04 and −0.59 mRy found in direct VASP calculations for 16- and 64-atom supercells, respectively, representing the random $Cu_{0.5}Zn_{0.5}$ alloy. The fact that the local relaxation energy in $Cu_{0.5}Zn_{0.5}$ is quite sensitive to both the size of the supercell and the number of k points in the Brillouin zone integration appears to be connected with the Fermi surface effects, which make the stoichiometric B2-CuZn unstable. In this respect the ETM model is certainly quite approximate. However, we believe that it still captures the energetics of the local relaxations with sufficient accuracy to make the high-temperature simulations meaningful. The inclusion of lattice relaxation effects in the end lowers the order-disorder transition temperature by about 100 K.

According to the existing phase diagram[59] the single-phase region of β-brass is shifted from the equiatomic composition by about 2 at. % towards Cu, and the order-disorder phase transition occurs at an off-stoichiometric composition. For this reason we have chosen the $Cu_{0.52}Zn_{0.48}$ alloy composition for the Monte Carlo simulations and recalculated the SGPM interactions. The new interactions are, in fact, very close to those at the equiatomic composition. In the Monte Carlo simulations we have included the 17 strongest interactions up to the 30th coordination shell, and used a $24\times24\times24$ simulation box based on the bcc lattice. In Fig. 8 we present the results for the configurational specific heat and the Warren-Cowley short-range order parameter at the first coordination shell. The calculated transition temperature of 780 K is only 40 K higher than the experimental data. This is a very good result taking into account the fact that the local relaxation energy is slightly underestimated in the ETM and that the vibrational free energy is completely neglected.

VI. ORDERING IN CUAU

Face-centered cubic CuAu alloys present a very interesting and instructive case regarding the comparison between different alloy theories. The Cu–Au phase diagram is relatively simple. It consists of the high-temperature random phase in the whole concentration range and three ordered phases: Cu_3Au, CuAu, and Au_3Cu. The structures of the Cu_3Au and the CuAu phases which are $L1_2$ and $L1_0$, respectively, are well established experimentally as well as theoretically. However, first-principles calculations disagree with the existing interpretations of the experimental data for the ground-state structure of Au_3Cu.[6,60] There is also a medium-temperature CuAu-II phase around the equiatomic composition, which is a long-period superstructure based on the $L1_0$ ordered phase.[61–63] The stabilization of this phase has most probably a statistical origin coupled with local lattice relaxations near antiphase boundaries, which leads to specific local disordering.[64] Energetically this is a very small effect which cannot be described on the basis of the usual effective interactions alone, and it is therefore not considered here.

The phase diagram and the ordering of Cu–Au alloys have been investigated intensively by first-principles theoretical methods (see Ref. 60 and references therein), which in almost all cases have been based on the use of the structure inverse method with different types of cluster expansions. In particular, the so-called mixed-space cluster expansion (MSCS) has been used by Zunger and co-workers[6,60,65] in recent calculations of the order-disorder phase transitions, SRO parameters, and ground-state structures in this system. In all these studies the Hamiltonian has been generated by a mapping of the enthalpies of formation of structures taken

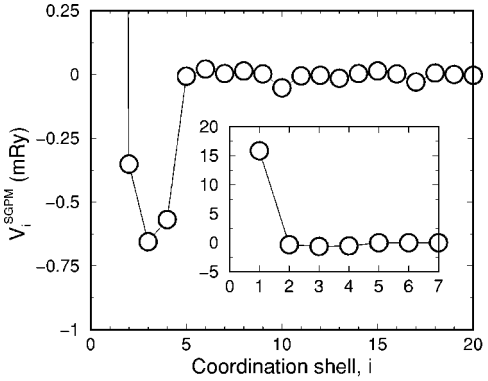

FIG. 9. SGPM pair interactions in $Cu_{0.75}Au_{0.25}$.

from the whole concentration range, which have been relaxed both in terms of volume and atomic positions. The effective interactions that result[6,60] from this procedure show substantial 3- and 4-site cluster interactions which leave the convergence of the corresponding expansion somewhat in doubt. Since both Cu and Au have only one *s* electron participating in the bonding (3*d*- and 5*d* shells being almost filled), it is difficult to imagine where the strong noncentral forces signaled by the 3- and 4-site interactions may have their *physical* origin.

The SGPM yields quite a different picture of the interactions in Cu–Au. In Fig. 9 we show the effective pair SGPM interactions calculated for a $Cu_{0.75}Au_{0.25}$ alloy, and it is clearly seen that the nearest-neighbor term dominates all other terms. Furthermore, the multisite interactions are very small, the largest being −0.31 mRy for the triangle of the nearest neighbors and 0.14 mRy for the triangle formed by two nearest-neighbor sites and a site at the third coordination shell. All other 3- and 4-site interactions are smaller by one order of magnitude or more.

To explain how the structure inverse method can lead to substantial 3- and 4-site interactions, we show in Fig. 10 the concentration and volume dependence of the nearest-neighbor pair interaction. For a fixed volume one notes that the concentration dependence of V_1 is very weak and linear. However, the dependence on volume is extremely strong, and one can clearly see that it originates from the screened Coulomb interactions due to a drastic change in the effective charge transfer with the volume. In the figure we have further indicated the range of the equilibrium Wigner-Seitz radii in the whole concentration range for CuAu. It is now clear that if the structure inverse method is used for the whole concentration range with the relaxed structures, the strong volume dependence of the effective pair interactions will have to be represented by higher-order concentration- and volume-independent interactions.

The present SGPM pair interactions reproduce quite well the ordering energy of $L1_2$-Cu_3Au (S_{WS}=2.8 a.u.): −7.05 mRy, which should be compared with the value from direct total energy calculations of −6.52 mRy, the total energy of a random $Cu_{0.75}Au_{0.25}$ alloy having been obtained by the LSGF method.[26,27] Although the SGPM interactions slightly overestimate the ordering energy of the L12 phase,[66] they reproduce very accurately the relative energies E_{LPSm}

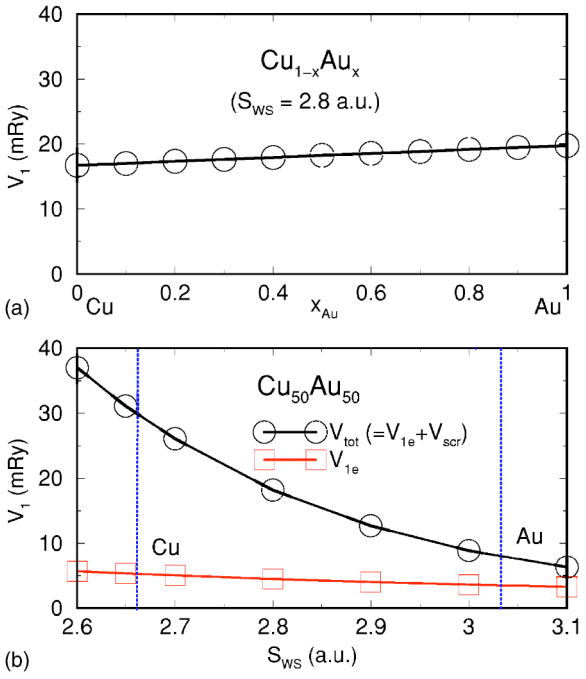

FIG. 10. (Color online) Concentration (a) and volume (b) dependence of nearest-neighbor SGPM interaction in CuAu. Concentration dependence calculated at fixed Wigner-Seitz radius of 2.8 a.u., while the volume dependence is determined for equiatomic alloy composition. The range of equilibrium Wigner-Seitz radii in CuAu alloys is indicated by vertical broken lines.

$[\equiv E_{LPS}(1x0)] - E_{L1_2}[\equiv E_{LPS}(100)]$ of the $L1_2$-based long-period superstructures (LPS*m*) as shown in Fig. 11, which are of the order of meV. The LPS possess a superstructure vector given by $2\pi/a(1x0)$, where x is determined by the modulation length m as $x=1/2m$. (A thorough description of such structures may be found in Ref. 1.) It is also interesting to notice that FP-LAPW results taken from Ref. 60 and the KKR-ASA(+M) results are in perfect agreement. The latter result is also very important, since the accuracy of the GPM

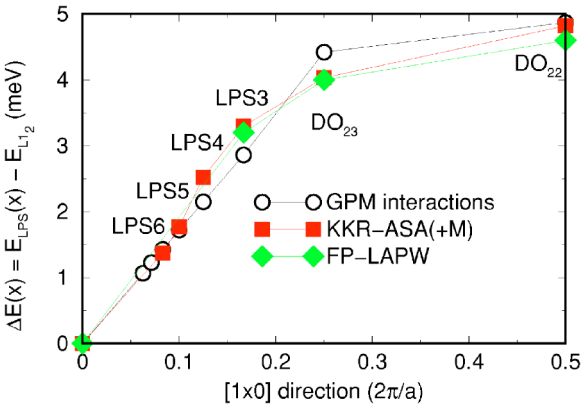

FIG. 11. (Color online) The energies of LPS(m) in Cu_3Au, as a function of the superstructure vector $\mathbf{k}=2\pi/a(1x0)$ ($x=1/2m$, where m is the modulation length), relative to the energy of the $L1_2$ structure ($\mathbf{k}=0$). The results of direct calculations: KKR-ASA(+M) are from this work, FP-LAPW from Ref. 60. DO_{22} and DO_{23} correspond to the LPS1 and LPS2, respectively.

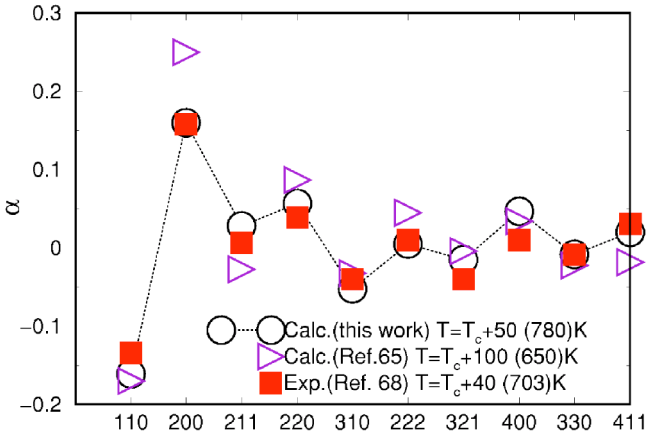

FIG. 12. (Color online) The Warren-Cowley SRO parameters in $Cu_{0.75}Au_{0.25}$ above order-disorder phase transition.

interactions is provided by the accuracy of the underlying first-principles method, and in this case apparently none of the approximations used in the KKR-ASA(+M) calculations has a significant impact on the final accuracy.

Using the SGPM interactions in a Monte Carlo simulation of a $Cu_{0.75}Au_{0.25}$ alloy, we find the order-disorder transition temperature T_0 to be 740 K. Once again we have added the local relaxation term given by the effective tetrahedron model (ETM).[28] As expected for an alloy with a large size mismatch, the effect of local relaxations on the transition temperature is significant. If we exclude the relaxation term we find T_0 to be at 1275 K. Although our transition temperature is slightly higher than the experimental value, we have included no term in the Hamiltonian to describe lattice vibrations. According to Ref. 60 such a term may lower T_0 by approximately 100 K.

There is one further point connected with the strong local relaxations and the approximation used for the exchange-correlation energy. As is well-known, there is no single approximation that works well for both of the two components of CuAu.[28,32,67] The GGA works well for the ground-state lattice parameter of the 3*d* metals but less well for the 5*d* metals, while the LDA does the opposite. As a result, the calculated relaxation energy of the CuAu alloy depends on the functional, the values being −51, −42, and −38 meV for LDA, LAG, and GGA, respectively. This effect is to some extent compensated by the volume dependence of the strength of the effective interactions, which shows the reverse trend being strongest for the GGA. However, such an uncontrolled compensation is hardly desirable.

In Fig. 12 we compare the SRO parameters in $Cu_{0.75}Au_{0.25}$ as calculated by Monte Carlo simulations based on our SGPM interactions with the experimental values obtained by Butler *et al.*[68] at about 40 K above the order-disorder transition temperature. Also shown are the results of Wolverton *et al.*[65] calculated by the Monte Carlo technique but with a MSCE Hamiltonian obtained using the SIM. The agreement with experiment is rather good (although we find reasonable but worse agreement at the other stoichiometries[69]).

This encouraged us to search for the experimentally observed temperature-dependent *X*-point splitting in the diffuse scattering intensity, which can be related to the Fourier transform of the SRO parameters. We observe no such splitting which was, in fact, seen in the MC simulations of Wolverton *et al.*[65,70] The latter authors ascribed the effect to entropy, which may induce a certain type of long-range SRO excitations due to specifically shallow energy landscape near the minimum in the reciprocal space. In other words, the necessary condition for a temperature-dependent shift is the existence of a quite shallow minimum in the ordering energy of the LPS, E_{LPSm}, close to the *X* point at $x=0$ $(m=\infty)$ which corresponds to the $L1_2$ structure.

Such a shallow minimum is indeed found in the mixed-space cluster-expansion representation of the $\Delta E(x) = E_{LPS}(1x0) - E_{L1_2}$ as seen, for instance, in Fig. 6 in Ref. 65. This is in contrast to the present results shown in Fig. 11, where the energy $\Delta E(x)$ increases steeply near the *X* point. It is not clear why the difference between the SGPM and MSCE-SIM results close to the *X* point arises. However, since the SGPM accurately reproduces the ordering energies of the LPS obtained by direct calculation in the KKR-ASA(+M), and as these in turn agree well with the direct FP-LAPW calculations of Ref. 65, we believe that the physical origin of this interesting effect is at present still an unresolved issue.

VII. LONG-PERIOD SUPERSTRUCTURES IN $Cu_{0.75}Pd_{0.25}$

In the Cu–Au system the number of terms in a Hamiltonian at a fixed volume and concentration is rather small and all the terms are short-ranged. In this section we shall consider the system of Cu-rich CuPd alloys that show exactly the opposite behavior. This system is well-known for the formation of long-period superstructures[71] based on the $L1_2$ ordered phase and for the related strong concentration dependence of the splitting at the *X* point in the diffuse scattering measurements on the disordered alloy.[72] Many of the interesting features in the thermodynamics of this system, including the two mentioned above, have been explained successfully on the basis of Fermi surface nesting arguments.[74,75] A strong and composition-dependent nesting of the Fermi surface has long been predicted and has recently been confirmed in positron annihilation studies.[73]

The Fermi surface nesting leads to an increase in the electronic susceptibility at the nesting vector, which in the $S^{(2)}$ formalism manifests itself as a peak in the Fourier transform of the pairwise interactions in the XW line of the Brillouin zone.[76] In a real-space theory such as the GPM, this is expected to lead to a long-range oscillatory form for the pairwise interactions in the direction of the nesting vector. That this is indeed the case is shown in Fig. 13, where we have plotted the SGPM interactions in the direction of the nesting vector [110] as well as along [100]. The former clearly exhibit oscillatory behavior and are longer ranged than the latter. Note that, although the interactions in the tail are very small in magnitude, they must be included in the Hamiltonian in order to reproduce the concentration dependence of the *X*-point splitting by Monte Carlo simulations.

The complex behavior of the concentration-dependent interactions is expected to cause problems in the construction

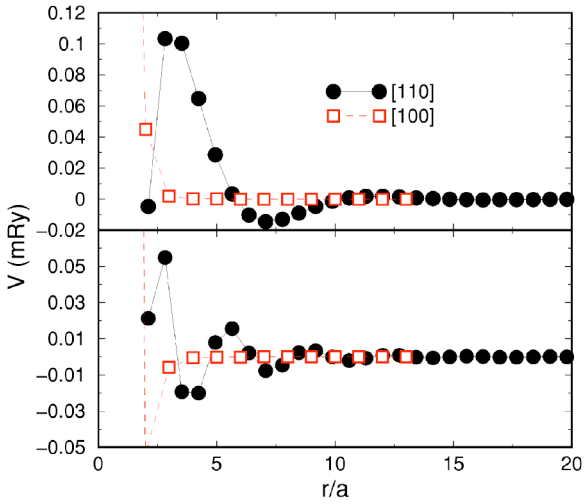

FIG. 13. (Color online) Pair interactions for $Cu_{0.75}Pd$ (top panel) and $Cu_{0.50}Pd$ (lower panel) shown in the [100] and [110] directions, the latter being the direction of the nesting vector.

of the concentration-independent interactions used in the SIM. Indeed, to the best of our knowledge, no SIM-based calculation has reproduced the concentration dependence of the *X*-point splitting or the concentration dependence of the LPS stability. However, the simulations by Lu *et al.*[77] exhibit a rather good agreement with the experimentally observed real-space SRO parameters in the first several coordination shells for a wide range of compositions. On the other hand, as we have seen in the case of the fcc CuZn system, these SRO parameters are likely to be dominated by the effective interactions in the first few shells, which presumably are easier to include in a SIM calculation than the long-ranged and complex concentration-dependent interactions that determine the concentration dependence of the *X*-point splitting.

So far we have only discussed effective pair interactions which, however, do not provide the complete physical picture in this system. Consider, for instance, Eq. (9), which shows that when $\tilde{g}_{ij}$ is large in the direction of the nesting vector, multisite interactions that involve vectors in the nesting direction one or more times may be important even for quite large distances between the sites. The dramatic effect of this mechanism is clearly seen in Fig. 14, where we show the energies of the LPSs at the stoichiometric 75% Cu composition. For this illustration, the SGPM Hamiltonian included 140 pair interactions, 44 3-site interactions, and a number of 4-site interactions. It is clear that without the multisite interactions one does not obtain a quantitative description of the LPS energetics in the CuPd system. Further, the fact that the minimum energy appears slightly shifted and becomes shallower with the inclusion of multisite interactions may be important in the determination of a quantitatively correct description of the diffuse scattering, where theory and experiment still show a discrepancy.[78]

The problem in the calculation of the LPS energetics is not simply the effect of some large three-site interactions, but is due to the large number of small yet finite 3-site interactions that must be included in the Hamiltonian. This is illustrated in Fig. 15, where we show the contribution from the

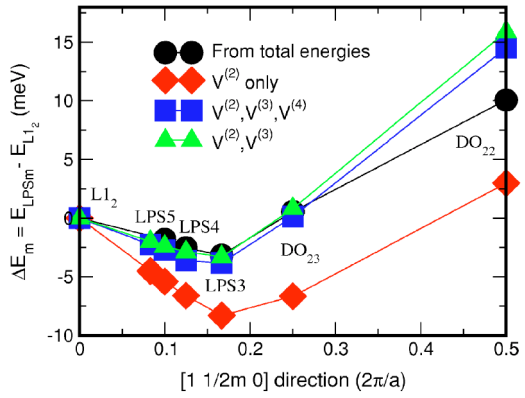

FIG. 14. (Color online) The energies of LPS*m* in Cu_3Pd as a function of the superstructure vector $\mathbf{k}=2\pi/a(11/2m0)$, relative to the energy of the $L1_2$ structure. Total energy calculations are done by the KKR-ASA(+M) method.

first 32 3-site interactions to the energies of LPS3($m=3$) and LPS4m($m=4$). At the starting point in the figure we plot the results of the summation of pair interactions alone. The following point, 111, is the result of adding the contribution to the ordering energy from interactions of the triangle of nearest neighbors. As one may see, these interactions do not contribute at all to the LPS energy in spite of the fact that they are the largest of the 3-site interactions.

It is clear that, although there are many 3-site interactions which are unimportant and may be omitted in the Hamiltonian, those that should be included are quite long-ranged and large in number. This causes problems both for the SIM and for the Monte Carlo simulations. In fact, the latter are slowed down considerably not only by the large number of 3-site interactions in the Hamiltonian but also by the large degeneracy of each of these interactions. For instance, the 3-site interactions labeled by 134, 137, and 337 have a degeneracy of 144. In Table I we show some of the most important 3-site interactions among those calculated. Although it is in general quite difficult to predict which multisite interaction will be important, we have found that the following simple rule usually works: The strongest multisite interac-

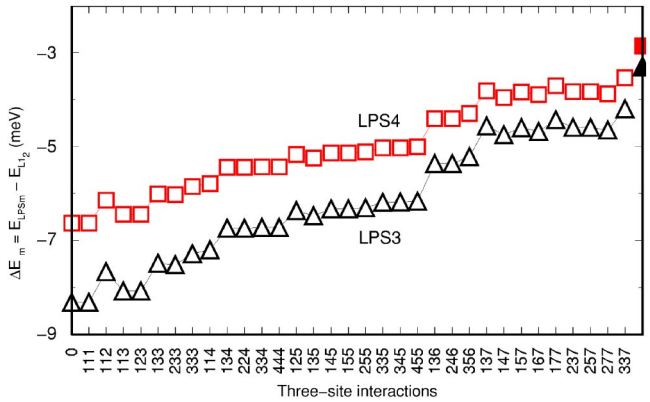

FIG. 15. (Color online) The relative energies of the LPS3 and LPS4 in Cu_3Pd as a function of the included 3-site interactions. The final point marks the final energy found by including all calculated (44) 3-site interactions.

TABLE I. Three-site interactions in $Cu_{0.75}Pd_{0.25}$ in concentration variables and (mRy). The number of equivalent clusters is given in square brackets.

111 [24]	112 [36]	113 [72]	133 [72]	333 [24]	134 [144]	224 [36]
0.727	−0.288	−0.091	0.065	0.051	−0.051	−0.065
125 [72]	136 [72]	137 [144]	1.4.10 [36]	1.10.17 [36]	4.4.17 [36]	1.17.30 [24]
−0.078	−0.088	0.036	−0.041	−0.053	−0.035	−0.032

tions are for those clusters which include the sides for which pair interactions have relatively high values compared to the others.

VIII. EFFECTIVE INTERACTIONS AND ORDERING TRANSITIONS IN PTCO

It is a major advantage of the GPM that it may be used in cases where the magnetic degrees of freedom are nontrivial. An instructive example of this is the Pt–Co system in which the Curie temperature drops monotonically from 1400 K in pure Co to zero in pure Pt.[79,80] As a result, the Curie temperatures of 700 and 350 K for random PtCo and Pt_3Co alloys, respectively, appear to be below the order-disorder transition temperatures which are 1100 and 1000 K for $L1_0$ -PtCo and $L1_2$-Pt_3Co, respectively. The disappearance of the global moment at the Curie temperature is due to a *disordering* of the direction of the local Co moments which, in fact, remain finite also above the Curie temperature. We therefore have a system in which the description by configurational thermodynamics of the paramagnetic state between the Curie temperature and the order-disorder transtion temperature must include nontrivial magnetic degrees of freedom.

In the most general case, this poses an extremely difficult problem as one must consider not only the separate chemical and magnetic degrees of freedoms (see Refs. 81–83 and references therein), but also the interplay between them. For instance, the local magnetic moment may depend in a complicated manner on the chemical environment, and in such a case a Hamiltonian consisting of independent Ising and Heisenberg terms describing the chemical and magnetic degree of freedom, respectively, will not be sufficient. Of course, it is possible in many cases to find simplified semiempirical models similar to that proposed in Ref. 84 for the calculation of the PtCo phase diagram, but the chemical and magnetic interactions in this type of Hamiltonian are difficult to identify and relate to first principles calculations. However, as we will show below, a full first-principles treatment can in fact be provided for this system.

The point is that if one is interested only in the "chemical" ordering between Pt and Co atoms above the Curie temperature, a much simpler approach can be used. This approach is based on the assumptions that the magnetic moments on Co atoms do not depend on their local chemical environment, i.e., on the number of the nearest-neighbor Pt atoms, and that they are in the disordered state. Such a state is quite well described by the disordered local moment (DLM) model, which assumes the existence on average of two types of Co atoms, one with spin up, $Co^{\uparrow}$, and the other with spin down, $Co^{\downarrow}$, which have the same concentration in the alloy and are distributed randomly relative to each other on the underlying lattice, whereby the average magnetic moment in the crystal will be zero. It follows that a binary Co_xPt_{1-x} alloy above the Curie temperature can be considered a three-component system: $Co^{\uparrow}_{x/2}Co^{\downarrow}_{x/2}Pt_{1-x}$ with a configurationally *uncorrelated* distribution of $Co^{\uparrow}$ and $Co^{\downarrow}$.

The pair interactions in such a ternary system will involve the exchange of a Co^x atom with a Pt atom in the presence of another Co^y atom, and can be defined as[85]

$$V(R)_{xy} \equiv V(R)_{\mathrm{Co}^x\mathrm{Co}^y} = v_{\mathrm{Co}^x\mathrm{Co}^y}(R) + v_{\mathrm{PtPt}}(R) - v_{\mathrm{Co}^x\mathrm{Pt}}(R) - v_{\mathrm{PtCo}^y}(R), \tag{17}$$

where $v_{AB}(R)$ is the interatomic potential between A and B atoms. However, since the spatial correlations of the purely magnetic configurations above the Curie temperature are small, we can reduce the problem to the case of a binary alloy by taking the average over effective interactions $V(R)_{xy}$ with different orientation of Co spins. Including now the symmetry of the spin up and spin down states, the effective pair interactions are

$$V(R) = \tfrac{1}{2}[V_{\uparrow\uparrow}(R) + V_{\uparrow\downarrow}(R)], \tag{18}$$

where $V(\mathbf{R})_{\uparrow\uparrow}$ and $V(\mathbf{R})_{\uparrow\downarrow}$ are the Pt–Co effective interactions which involve pairs of Co atoms with ferromagnetic and antiferromagnetic spin alignment, respectively. Multisite interactions may be obtained in a similar way but will not be given here.

It would clearly be a problem to derive effective interactions for the PtCo system by the SIM as the basis of input structures must be generalized to include also magnetic structures. However, increasing the degrees of freedom presents no problem for a perturbative method such as the GPM, and the coherent potential approximation is a natural tool for calculating the electronic structure of the DLM state. In the notations introduced in Sec. II we have for the one-electron part of the SGPM interaction

$$V^{GPM}_{xy}(R) = -\frac{1}{\pi}\,\mathrm{Im}\int^{E_F} \mathrm{Tr}(t^x\tilde{g}_{\mathbf{R}}t^y\tilde{g}_{-\mathbf{R}} + t^{\mathrm{Pt}}\tilde{g}_{\mathbf{R}}t^{\mathrm{Pt}}\tilde{g}_{-\mathbf{R}} - t^x\tilde{g}_{\mathbf{R}}t^{\mathrm{Pt}}\tilde{g}_{-\mathbf{R}} - t^{\mathrm{Pt}}\tilde{g}_{\mathbf{R}}t^y\tilde{g}_{-\mathbf{R}}), \tag{19}$$

where $t^x \equiv t^{\mathrm{Co}^x}$.

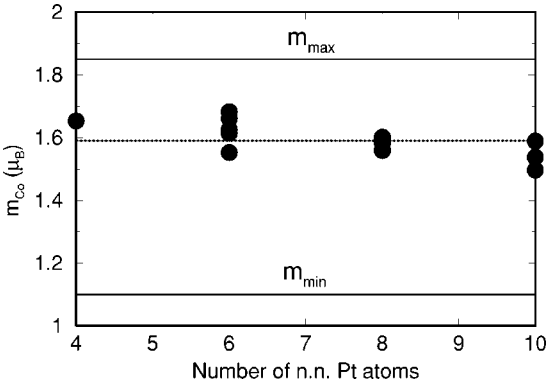

FIG. 16. Magnetic moment of Co atoms in a 384-atom supercell representing random $Pt_{0.5}Co^{\uparrow}_{0.25}Co^{\downarrow}_{0.25}$ alloy which have equal number of $Co^{\uparrow}$ and $Co^{\downarrow}$ atoms as a function of number of Pt atoms in the first coordination shell.

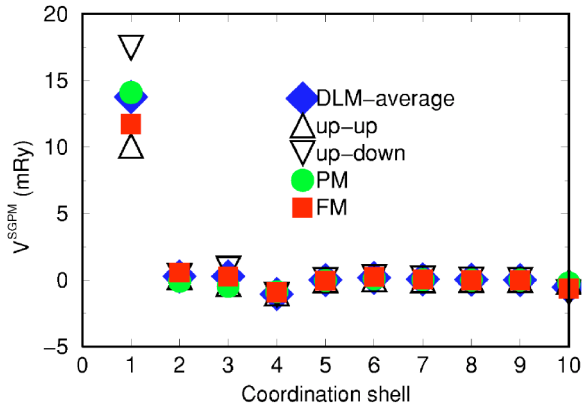

FIG. 17. (Color online) Pair SGPM interactions in $Co_{0.75}Pt_{0.25}$ obtained in the DLM, ferromagnetic (FM), and nonmagnetic calculations (PM).

The screened Coulomb interactions, $V_{scr}(\mathbf{R})$, do not depend on the direction of the spin and thus are the same for $V(\mathbf{R})_{\uparrow\uparrow}$ and $V(\mathbf{R})_{\uparrow\downarrow}$. Moreover, it is natural to assume that the screening is independent of the magnetic state, an assumption which we have confirmed by supercell calculations. Hence, the actual screened Coulomb interactions used were those obtained in a ferromagnetic $Pt_{0.75}Co_{0.25}$ alloy.

To test our assumptions regarding the screening in PtCo and the influence of the local environment on the magnetic state of the Co atoms, we have performed LSGF calculations for a 384-atom supercell of a DLM $Co^{\uparrow}_{0.25}Co^{\downarrow}_{0.25}Pt_{0.5}$ alloy having an exact relative random distribution of Pt, $Co^{\uparrow}$, and $Co^{\downarrow}$ atoms in the first three coordination shells (in coordination shells four to eight the SRO parameters were of the order of 0.01), and an exact relative random distribution of $Co^{\uparrow}$ and $Co^{\downarrow}$ atoms in the first two coordination shells. As a first result we find that the value of the on-site screening constant in the supercell DLM calculations is very close to that of a ferromagnetic alloy indicating that the screening in this alloy system is quite insensitive to the magnetic state.

Second, we find that the value of the magnetic moment of the Co atoms ranges from 1.10 to $1.85\mu_B$ depending on the average magnetic moment in the first coordination shell. In fact, the value increases if the average moment in the first coordination is ferromagnetically aligned and decreases otherwise. Finally, we find, as assumed above, that the magnetic moment of the Co atoms depends very little on the number of the nearest neighbor Pt atoms as may be seen in Fig. 16. This means that the decoupling of the chemical and magnetic interactions above the Curie temperature is indeed a reasonable approximation.

In Fig. 17 we show the calculated SGPM interactions for the $Pt_{0.75}Co_{0.25}$ alloy in three different magnetic states: Ferromagnetic, nonmagnetic, and DLM. It is seen that the average DLM interactions at the first coordination shell are very close to those of the nonmagnetic state. At more distant coordinations shells they deviate somewhat, however, and this turns out to be important in the description of the order-disorder transition. It is further seen that the nearest-neighbor interactions in the ferromagnetic alloy and $V(R_1)_{\uparrow\uparrow}$ are weaker than the average DLM and paramagnetic interactions, which means that ferromagnetism suppresses ordering. At the same time, $V(R_1)_{\uparrow\downarrow}$ involving Co atoms with antiferromagnetic alignment of the spins is substantially stronger than all other interactions. This is a natural effect in an alloy with pronounced ferromagnetic behavior, since the separation of two Co atoms with ferromagnetic spin alignment is energetically favorable relative to the separation of two Co atoms with antiferromagnetic spin alignment.

The results of MC simulations for $Pt_{0.75}Co_{0.25}$ with the three sets of interactions including the local lattice relaxation interactions determined in the ETM are shown in Table II. It is seen that the DLM interactions reproduce the experimental order disorder transition temperature to within 10 K while the nonmagnetic and the ferromagnetic interactions produce transition temperatures which are 200 and 400 K lower, respectively. Note that the latter is only 200 K above the Curie temperature at this composition. The success of our averaged DLM interactions indicates that the neglect of magnetic correlations assumed in this model is indeed reasonable. This should not be surprising since the order-disorder transition takes place 600 K above the Curie temperature. We conclude that, although a correct treatment of the magnetic state appears essential to construct a quantitatively accurate Hamiltonian for use in the alloy thermodynamics, magnetic correlations themselves are unimportant.

IX. MAGNETIC EXCHANGE INTERACTION PARAMETERS FROM THE GPM

The most widely used perturbation technique for obtaining exchange interaction parameters for a Heisenberg Hamiltonian is the Liechtenstien-Katsnelson-Gubanov method (LKGM),[86,87] which is based on the so-called magnetic force theorem. This theorem is applied to the system in ferromag-

TABLE II. Order-disorder transition temperatures in $Co_{0.25}Pt_{0.75}$ with interactions calculated from different reference states.

Nonmagnetic	DLM (average)	Ferromagnetic	Experiment
800 K	1030 K	600 K	1040 K

TABLE III. First several exchange parameters by the GPM and LKGM for bcc Fe at the lattice spacing 2.88 Å in meV. Electronic temperature in parenthesis.

	GPM			LKGM		
Shell	GGa (0 K)	LDA (0 K)	LDA (1000 K)	GGA (0 K)	LDA (0 K)	LDA (0 K)[a]
111	27.27	25.49	23.83	10.62	12.67	19.48
200	1.77	1.13	1.09	12.74	8.72	11.09
220	1.11	1.05	0.92	−0.31	−0.02	−0.21
311	0.40	0.27	0.20	−2.22	−1.60	−1.71
222	−2.56	−2.31	−2.11	−0.49	−0.74	−1.94
400	−0.33	−0.36	−0.38	0.22	0.27	0.84
331	−0.28	−0.32	−0.28	−0.39	−0.12	0.01
420	−0.01	−0.04	−0.03	0.14	0.11	0.20
422	−0.44	−0.42	−0.36	−0.02	−0.25	−0.44
333	1.18	1.24	1.12	2.66	1.93	2.54
511	−0.02	−0.01	−0.01	0.39	0.21	

[a]Reference 98, lattice spacing: 2.87 Å.

netic state, and exchange interactions are determined from a small-angle reorientation of two spins on different sites. As we will see below, this particular limit may induce some specific restrictions on the exchange interactions if they exhibit a pronounced angle dependence, so their application, for instance, to calculations of the Curie temperature may lead to inaccurate results.

It turns out that the opposite limit, which is a large-angle spin excitation, needed for a correct representation of the paramagnetic state, can be given by the GPM interactions obtained for the DLM state. This is true, at least, for a "Heisenberg system" where the dependence of the value of the magnetic moment on the configuration is small and the exchange interactions themselves do not depend on the underlying magnetic configuration, so collinear magnetic configurations should be described by the same exchange parameters as noncollinear configurations. Therefore, the problem of finding the magnetic interactions in a pure metal is reduced to the problem of calculating the ordinary effective interactions in the corresponding DLM alloy of "spin-up" and "spin-down" atoms. In this case, the GPM yields effective interactions which are simply (up to some coefficient depending on the form of the Hamiltonian) the Heisenberg exchange interaction parameters.

One can expect the GPM to be quite accurate in obtaining exchange interactions. In fact, the main approximation in the GPM is the CPA which, however, usually works very well for the DLM state. Furthermore, there is no problem with the screening since the spin-up and spin-down atoms are chemically equivalent, which means that there is no charge transfer effect upon a change of the direction of the spin. It should also be noted that the application of the GPM to the DLM alloy is equivalent to the method by Oguchi, Terakura, and Hamada (OTH),[88] in which the exchange parameters are obtained as the interaction energy between two magnetic moments in the DLM paramagnetic medium, the only difference being the use of the fully renormalized form for the exchange parameters by OTH.

The interaction parameters may, of course, be determined by the structure inverse method generalized to magnetically ordered systems (see, for instance, Refs. 89–92). However, the problems arising here are similar to those found in the application of the SIM in alloy calculations. Therefore, the purpose of this section is to demonstrate that the GPM is an accurate and powerful alternative to such methods in this case, too.

A. Curie temperature in bcc Fe

In the following we apply the LKGM and GPM in calculations of the Curie temperature for bcc Fe. This is a well-studied system and it has been subjected to numerous first-principles calculations, (see, for instance, Refs. 89 and 93), from the work by You *et al.*[94] to the most recent calculations by Bruno.[95] Here, we mention the calculations based on the DLM state by Staunton *et al.*,[96,97] which demonstrated that bcc Fe can be considered a Heisenberg system, and the calculations by Oguchi *et al.*[88] also based on the DLM, which gave a Curie temperature of 2700 K that is far above the experimental value of 1040 K. Since the GPM is formally equivalent to the method used by Oguchi *et al.*, it will be interesting to see how the GPM works in this case.

In Table III we present six sets of pair exchange interaction parameters J_{ij} for bcc Fe obtained by the GPM and the LKGM as defined by the Heisenberg Hamiltonian

$$H = -\sum_{ij} J_{ij}\mathbf{e}_i\mathbf{e}_j, \tag{20}$$

where $\mathbf{e}_i$ is a unit vector in the direction of the local magnetic moment at site i. All calculations used a lattice spacing of 2.88 Å close to the experimental value at 1000 K except those of Ref. 98, which used the room temperature value. We note that the effect of the exchange-correlation approximation is rather small and, in fact, much smaller than the difference between the GPM and LKGM exchange parameters, which is clearly a qualitative difference.

TABLE IV. Curie temperature in bcc Fe obtained with different sets of the pair exchange interaction parameters.

El. temperature	LKGM (GGA)	LKGM ((LDA)	GPM ((GGA)	GPM ((LDA)	Experiment
0 K	560 K	640 K	1330 K	1180 K	
1000 K	700 K	740 K	1260 K	1090 K	1040 K

The results in the third column of Table III includes an electronic temperature of 1000 K in the Fermi-Dirac distribution in the self-consistent electronic-structure and exchange-parameter calculations. It is seen from the LDA data in the table that an increase in the electronic temperature lowers the exchange interactions, which subsequently will lead to a lower Curie temperature. In our LKGM calculations, not shown in the table, the effect is opposite, i.e., an increase in the electronic temperature increases the exchange parameters in the first coordination shell, leading to a higher Curie temperature.

In Table IV we show the Curie temperatures obtained by Monte Carlo simulations using a Heisenberg Hamiltonian[99] with different sets of pair exchange interaction parameters and two electronic temperatures of 0 and 1000 K. It is seen that the GPM-LDA exchange parameters yield Curie temperature closest to the experimental value, overestimating it by only 50 K, while the GPM-GGA calculations overestimate it by 220 K. It is interesting to note that the effect of the exchange-correlation approximation on the Curie temperature is opposite in sign and much smaller in the LKGM calculations than in the GPM calculations. We also find that if the electronic temperature in the GPM calculations is lowered to 0 K the Curie temperature increases by approximately 100 K in the subsequent Monte Carlo simulations, while the same lowering of the electronic temperature has the opposite effect on the LKGM exchange parameters and Curie temperature.

The results in Table IV show that the GPM works quite well for the exchange parameters and the Curie temperature, while our LKGM pair exchange parameters yield Curie temperatures that are too low. This apparent failure of the LKGM is quite unexpected, since most of the previous LKGM calculations of the Curie temperature in bcc Fe are in good agreement with the experimental data. To the best of our knowledge there is only one exception: The calculations by Antropov *et al.*,[100] who, using LKGM exchange parameters in spin-dynamics simulations, found the ferromagnetic transition in bcc Fe to be about 600 K. Furthermore, in a recent study based on the LKGM exchange parameters obtained by Pajda *et al.*[98] and the random phase approximation, Bruno[95] found the Curie temperature to be 950 K, which upon a renormalization due to a transverse magnetic field increased to 1057 K, in perfect agreement with experiment.

Obviously, a discrepancy of the order of 300 K in the Curie temperature obtained by what should be the exact same LKGM approach needs an explanation. From a comparison of the two last columns in Table III it is immediately clear that the discrepancy is caused by the quite substantial difference between the present LKGM exchange parameters and those obtained by Pajda *et al.*[98] We shall now clarify the origin of this difference by showing what is required to reproduce the exchange parameters by Pajda *et al.*[98]

First we note that the calculations by Pajda *et al.* have been performed at the room temperature lattice spacing, which we assume to be 2.87 Å. However, this is not the cause of the difference since our LKGM exchange parameter at the first coordination shell calculated at this lattice spacing is only 0.64 meV higher than the value in Table III. We then decreased the accuracy of the electronic structure calculations used to obtain the LKGM exchange parameters by introducing the approximations used by Pajda *et al.* That is, we used the LMTO parametrization of the potential function, not the exact KKR one, and instead of an *spdf* basis we used an *spd* basis. Finally, we turned off the relativistic effects. We find the LKGM exchange parameters obtained in this way in the first four shells to be 18.61, 10.10, −0.06, and −1.73 [meV], respectively, which within a few percent reproduces the values shown in the last column of Table III.

Thus, the LKGM exchange parameters obtained by Pajda *et al.*[98] are based on one in appropriate approximation, neglect of relativistic effects, and more approximate electronic structure calculations. The successful calculation of the Curie temperature in bcc Fe by Pajda *et al.*[98] and subsequently by Bruno[95] is fortuitous. With the present LKGM exchange parameters the latter author would have found a Curie temperature of about 850 K including the renormalization due to a transverse magnetic field.[95,101–103]

One of the advantages of the GPM method is that it allows one to determine high-order terms of the Heisenberg Hamiltonian straightforwardly. It turns out that such terms give quite substantial contribution to the Curie temperature of the bcc Fe, the strongest interactions of which we have found to be (i) the biquadratic exchange parameters, $J_{ij}^{(2-2)}$ which enter the Hamiltonian as $-\Sigma_{ij}J_{ij}^{(2-2)}(\mathbf{e}_i\mathbf{e}_j)^2$ for the first two coordination shells and which are −0.56 and 0.19 meV, respectively, and (ii) the 4-site exchange parameter, $J_{ijlk}^{(4)}$ which enters the Hamiltonian as $-1/3\Sigma_{ijkl}J_{ijlk}^{(4)}[(\mathbf{e}_i\mathbf{e}_j)(\mathbf{e}_k\mathbf{e}_l)+(\mathbf{e}_i\mathbf{e}_k)(\mathbf{e}_j\mathbf{e}_l)+(\mathbf{e}_i\mathbf{e}_l)(\mathbf{e}_j\mathbf{e}_k)]$ (Ref. 104) for the tetrahedron consisting of four nearest-neighbor sides and two next-nearest-neighbor sides and which is −0.73 meV (LDA, $T=1000$ K). From the sign convention it is clear that these exchange parameters should reduce the stability of the ferromagnetic state, and indeed the Curie temperature drops by approximately 50 K when they are included in the Heisenberg MC simulations. This brings the theoretical GPM-LDA result into perfect agreement with the experimental data while the GPM-GGA result is still off by 150 K, i.e., 15% off the experimental value.

Since higher order terms have been found to be important in the calculation of the Curie temperature of fcc Fe within the GPM, there is a strong possibility that such terms are also important in the LKGM. This, together with renormalization of the LKGM interactions,[95,101] could increase the Curie temperature in the case of the LKGM; however, the investigation of this point is beyond the scope of the present paper.

B. Spin spirals in bcc Fe

As has been mentioned at the beginning of this section, the LKGM exchange interactions, being determined from a

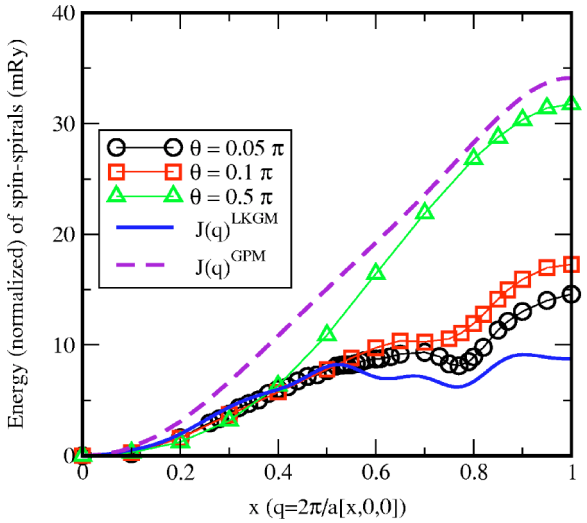

FIG. 18. (Color online) The energy of spin spirals in bcc Fe in the Γ-H direction of the Brillouin zone obtained in the direct KKR-ASA spin-spiral calculations for three different azimuthal tilt θ and from pair GPM and LKGM exchange parameters.

low-angle spin perturbation, may easily fail in the calculations of the Curie temperature, which is most probably the case of bcc Fe. On the other hand, it has been noticed (see, for instance, Ref. 92) that the LKGM interactions in fact reproduce quite well the magnon spectrum, obtained in the direct total energy calculations of low-angle spin spirals. Besides, by definition it should also produce quite well the long-wave limit.[101] In this view one can argue that the success of the GPM exchange interaction parameters is accidental, since it cannot be such that both methods are accurate; the interactions and the results for the Curie temperature are quite different.

To show that this is not the case we present in Fig. 18 the calculated energies of spin spirals in bcc Fe done for three different azimuthal angles: $\theta=0.05\pi$, 0.1π, and 0.5π together with the Fourier transform of the pair GPM and LKGM exchange interaction parameters (first 50 and 160 coordination shells have been used, respectively), $J(q)$, in the Γ-H direction of the bcc Brillouin zone. In the pair-interaction Heisenberg model the energy of a spin spiral is given by $J(q)\sin^2\theta$, and therefore to be able to compare all the results we have normalized all the energies obtained in the direct calculations by $1/\sin^2\theta$.

It is seen that there is a substantial difference between the energies of spin spirals for different θ, which can be due to (1) higher order interactions and/or (2) deviation of the magnetic behavior of Fe from the Heisenberg model (which, of course, also includes higher order terms). The energy of spin spiral obtained for $\theta=0.5\pi$ exhibits very smooth monotonic behavior, which is similar and close to the $J(q)$ obtained from the GPM exchange interaction parameters.

It is also clear that $J(q)$ obtained from the LKGM exchange interaction parameters very well reproduce the energy of spin spirals in the long-wave limit (small **q**), and for $\theta\rightarrow 0$. One can clearly see the appearance of the nonmonotonic behavior of spin spirals in the case of the LKGM, which some associate with Kohn-type anomalies. That is, we indeed have the case where both the GPM and LKGM interactions work quite well, but each one in its own well-defined limit. Taking into consideration the fact that the paramagnetic state corresponds to the large-angle limit, it is quite natural to expect good GPM results for the Curie temperature in bcc Fe.

X. SUMMARY

We have demonstrated that the generalized perturbation method (GPM), introduced into alloy theory more than a quarter of a century ago, can provide both a quantitatively accurate as well as physically transparent framework for the investigation of problems in alloy systems. Further, we have shown that the theory allows an easy extension to cases where magnetic degrees of freedom are important. Indeed, as a limiting case of this we have calculated the exchange parameters for Fe and found that they give a good description of this itinerant ferromagnet.

As regards the comparison with other alloy theories such as the structure inverse method (SIM), we wish to bring into focus the fact that the theories are to a large degree *complementary*. For example, in the GPM one can systematically search for the types and ranges of interactions that are important, whereas in the SIM this fact must be guessed at or allowed to "emerge" (rather unreliably, as we have seen) from the fitting process. On the other hand, the accuracy of the SIM is in principle limited only by the accuracy of the particular DFT used, whereas the GPM relies on the essentially uncontrolled approximations of the CPA and ASA geometry. However, the GPM is expected to be accurate for long-range interactions, and so the SIM could be used to confidently correct for errors in the earlier coordination shells. One can make the further point that the GPM will, by its perturbative nature, always be more efficient in highly inhomogeneous situations, or where the number of types of degrees of freedom is large, whereas it is only through the SIM that the contribution of, e.g., long-range elastic forces to the effective interactions may be determined.

To conclude, we have shown that the GPM can, in many cases, provide both a quantitatively accurate as well as physically transparent effective interaction. However, our hope is not to establish the GPM as a stand-alone alternative to the SIM, but rather to point out the complementary aspects of both theories, and perhaps encourage studies in which both approaches may be fruitfully combined.

[1] F. Ducastelle, *Order and Phase Stability in Alloys* (North-Holland, Amsterdam, 1991).
[2] A. G. Khachaturyan, *Theory of Structural Transformations in Solids* (Wiley, New York, 1983).
[3] D. de Fontaine, in *Solid State Physics*, edited by H. Erenreich, F. Seitz, and D. Turnbull (Academic, New York, 1979), Vol. 2, p. 117.
[4] J. W. D. Connolly and A. R. Williams, Phys. Rev. B **27**, 5169 (1983).
[5] A. Zunger, in *NATO ASI on Statics and Dynamics of Alloy Phase Transformations* (Plenum Press, New York, 1994), p. 361.
[6] A. Zunger, L. G. Wang, G. S. W. Hart, and M. Sanati, Modell. Simul. Mater. Sci. Eng. **10**, 685 (2002).
[7] R. Drautz, H. Reichert, M. FÄhnle, H. Dosch, and J. M. Sanchez, Phys. Rev. Lett. **87**, 236102 (2001).
[8] F. Ducastelle and F. Gautier, J. Phys. F: Met. Phys. **6**, 2039 (1976).
[9] P. Soven, Phys. Rev. **156**, 809 (1967).
[10] D. W. Taylor, Phys. Rev. **156**, 1017 (1967).
[11] S. Kirkpatrick, B. Velicky, and H. Erenreich, Phys. Rev. B **1**, 3250 (1970).
[12] A. Gonis, X.-G. Zhang, A. J. Freeman, P. Turchi, G. M. Stocks, and D. M. Nicholson, Phys. Rev. B **36**, 4630 (1987).
[13] P. E. A. Turchi, G. M. Stocks, W. H. Butler, D. M. Nicholson, and A. Gonis, Phys. Rev. B **37**, 5982 (1988).
[14] V. Drchal, J. Kudrnovský, L. Udvardi, P. Weinberger, and A. Pasturel, Phys. Rev. B **45**, 14 328 (1992).
[15] P. P. Singh and A. Gonis, Phys. Rev. B **47**, 6744 (1993).
[16] A. V. Ruban and H. L. Skriver, Phys. Rev. B **66**, 024201 (2002).
[17] A. V. Ruban, S. I. Simak, P. A. Korzhavyi, and H. L. Skriver, Phys. Rev. B **66**, 024202 (2002)
[18] A. R. Mackintosh and O. K. Andersen, in *Electrons at the Fermi Surface*, edited by M. Springford (Cambridge University Press, Cambridge, 1980).
[19] J. M. Sanchez, F. Ducastelle, and D. Gratias, Physica A **128**, 334 (1984).
[20] D. G. Pettifor, *Bonding and Structure of Molecules and Solids* (Clarendon Press, Oxford, 1995).
[21] A. E. Carlsson, in *Solid State Physics*, edited by H. Erenreich, F. Seitz, and D. Turnbull (Academic, New York, 1990), Vol. 43, p. 1.
[22] W. Schweika and A. E. Carlsson, Phys. Rev. B **40**, 4990 (1989).
[23] M. Asta, C. Wolverton, D. de Fontaine, and H. Dryesseé, Phys. Rev. B **44**, 4907 (1991).
[24] R. Monnier, Philos. Mag. B **75**, 67 (1997).
[25] A. Gonis, P. P. Singh, and P. E. A. Turchi, in *NATO ASI on Metallic Alloys: Experimental and Theoretical Perspectives* (Kluwer Academic, Dordrecht, 1994), p. 197.
[26] I. A. Abrikosov, A. M. N. Niklasson, S. I. Simak, B. Johansson, A. V. Ruban, and H. L. Skriver, Phys. Rev. Lett. **76** 4203 (1996).
[27] I. A. Abrikosov, S. I. Simak, B. Johansson, A. V. Ruban, and H. L. Skriver, Phys. Rev. B **56**, 9319 (1997).
[28] A. V. Ruban, S. I. Simak, S. Shallcross, and H. L. Skriver, Phys. Rev. B **67**, 214302 (2003).
[29] A. V. Ruban and H. L. Skriver, Comput. Mater. Sci. **15**, 119 (1999).
[30] N. E. Christensen and S. Satpathy, Phys. Rev. Lett. **55**, 600 (1985).
[31] J. P. Perdew and Y. Wang, Phys. Rev. B **45**, 13 244 (1992).
[32] L. Vitos, B. Johansson, J. Kollar, and H. L. Skriver, Phys. Rev. A **61**, 052511 (2000); Phys. Rev. B **62**, 10 046 (2000).
[33] Y. Wang and J. P. Perdew, Phys. Rev. B **44**, 13 298 (1991); J. P. Perdew, J. A. Chevary, S. H. Vosko, K. A. Jackson, M. R. Pederson, D. J. Singh, and C. Fiolhais, *ibid.* **46**, 6671 (1992).
[34] H. J. Monkhorst and J. D. Pack, Phys. Rev. B **13**, 5188 (1972).
[35] G. Kresse and J. Hafner, Phys. Rev. B **48**, 13 115 (1993).
[36] G. Kresse and J. Furthmüller, Comput. Mater. Sci. **6**, 15 (1996); Phys. Rev. B **54**, 11 169 (1996).
[37] P. E. Blöchl, Phys. Rev. B **50**, 17 953 (1994).
[38] G. Kresse and D. Joubert, Phys. Rev. B **59**, 1758 (1999).
[39] C. Barret and T. B. Massalski, *Structure of Metals* (Pergamon, Oxford, 1980).
[40] A. T. Paxton, M. Methfessel, and D. G. Pettifor, Proc. R. Soc. London, Ser. A **453**, 1493 (1997).
[41] U. Haussermann and S. I. Simak, Phys. Rev. B **64**, 245114 (2001).
[42] G. M. Stocks, W. M. Temmerman, and B. L. Györffy, Phys. Rev. Lett. **41**, 339 (1978).
[43] J. S. Faulkner and G. M. Stocks, Phys. Rev. B **23**, 5628 (1981).
[44] D. D. Johnson, D. M. Nicholson, F. J. Pinski, B. L. Gyorffy, and G. M. Stocks, Phys. Rev. Lett. **56**, 2088 (1986).
[45] D. D. Johnson, D. M. Nicholson, F. J. Pinski, B. L. Gyorffy, and G. M. Stocks, Phys. Rev. B **41**, 9701 (1990).
[46] D. D. and Johnson, F. J. Pinski, Phys. Rev. B **48**, 11 553 (1993).
[47] P. E. A. Turchi, M. Sluiter, F. J. Pinski, D. D. Johnson, D. M. Nicholson, G. M. Stocks, and J. B. Staunton, Phys. Rev. Lett. **67**, 1779 (1991); **68**, 418 (1992).
[48] B. Magyari-Kope, G. Grimvall, and L. Vitos, Phys. Rev. B **66**, 064210 (2002).
[49] S. Muller and A. Zunger, Phys. Rev. B **63**, 094204 (2001).
[50] The 3- and 4-site interactions are practically negligible in this system. We found that the strongest is a 3-site interaction for the triangle of the nearest neighbors, which is 0.05 mRy, all others being almost an order of magnitude less. Furthermore, this interaction gives exactly the same contribution to the ordering energies of the DO_{22}, DO_{23}, and $L1_2$ structures.
[51] L. Reinhard, B. Schonfeld, G. Kostorz, and W. Buhrer, Phys. Rev. B **41**, 1727 (1990).
[52] L. Reinhard, B. Schonfeld, G. Kostorz, and W. Buhrer, Z. Metallkd. **84**, 251 (1993).
[53] V. L. Moruzzi, J. F. Janak, and K. Schwarz, Phys. Rev. B **37**, 790 (1988).
[54] P. A. Korzhavyi, A. V. Ruban, S. I. Simak, and Yu. Kh. Vekilov, Phys. Rev. B **49**, 14 229 (1994).
[55] W. B. Pearson, *A Handbook of Lattice Spacings and Structures of Metals and Alloys* (Pergamon, New York, 1958).
[56] J. Als-Nielsen and O. W. Dietrich, Phys. Rev. **153**, 706 (1967).
[57] O. W. Dietrich and J. Als-Nielsen, Phys. Rev. **153**, 711 (1967).
[58] A. V. Ruban (unpublished).
[59] T. B. Massalski, *Binary Alloy Phase Diagrams* (ASM International, Materials Park, OH, 1990).
[60] V. Ozolins, C. Wolverton, and A. Zunger, Phys. Rev. B **57**, 6427 (1998).
[61] C. H. Johansson and J. O. Linde, Ann. Phys. (Leipzig) **25**, 1 (1936).
[62] D. Watanabe and K. Takashima, J. Appl. Crystallogr. **8**, 598 (1975).
[63] M. Gyumont, R. Portier, D. Gratias, Acta Crystallogr., Sect. A: Found. Crystallogr. **36**, 792 (1980).

[64] A. T. Paxton and H. M. Polatoglou, Phys. Rev. Lett. **78**, 270 (1997).
[65] C. Wolverton, V. Ozolins, and A. Zunger, Phys. Rev. B **57**, 4332 (1998).
[66] The main source of error in this case is probably inaccuracy in the determination of the intersite screening constants for the screened Coulomb interactions, especially for the first coordination shell, since they are calculated within the geometry of the atomic sphere approximation. Such an error may become substantial in systems like CuAu, where the alloy components have a large size mismatch, and therefore large effective charge transfer.
[67] A. Khein, D. J. Singh, and C. J. Umrigar, Phys. Rev. B **51**, 4105 (1995).
[68] B. D. Butler and J. B. Cohen, J. Appl. Phys. **65**, 2214 (1988).
[69] S. Shallcross (unpublished).
[70] V. Ozolins, C. Wolverton, and A. Zunger, Phys. Rev. Lett. **79**, 955 (1997).
[71] G. Ceder, D. de Fontaine, H. Dreyssé, D. M. Nicholson, G. M. Stocks, and B. L. Györffy, Acta Metall. Mater. **38**, 2299 (1990).
[72] K. Sato, D. Watanabe, and S. Ogawa, J. Phys. Soc. Jpn. **17**, 1647 (1962); H. Reichert, S. C. Moss, and K. S. Liang, Phys. Rev. Lett. **77**, 4382 (1996); X. Wang, K. F. Ludwig, Jr., O. Malis, J. Mainville, X. Flament, and R. Caurdon, Phys. Rev. B **63**, 092201 (2001).
[73] I. Wilkinson, R. J. Hughes, Zs. Major, S. B. Dugdale, M. A. Alam, E. Bruno, B. Ginatempo, and E. S. Giuliano, Phys. Rev. Lett. **87**, 216401 (2001).
[74] S. C. Moss, Phys. Rev. Lett. **22**, 1108 (1969).
[75] B. L. Györffy and G. M. Stocks, Phys. Rev. Lett. **50**, 374 (1983).
[76] R. V. Chepulskii, J. B. Staunton, Ezio Bruno, B. Ginatempo, and D. D. Johnson, Phys. Rev. B **65**, 064201 (2001).
[77] Z. W. Lu, D. B. Laks, S.-H. Wei, and A. Zunger, Phys. Rev. B **50**, 6642 (1994).
[78] I. Tsatskis and E. K. H. Salje, J. Phys.: Condens. Matter **10**, 3791 (1998).
[79] J. Crange and D. Pearsons, Proc. R. Soc. London, Ser. A **25**, 509 (1960).
[80] J. Crange and W. R. Scott, J. Appl. Phys. **36**, 921 (1965).
[81] J. M. Sanchez and C. H. Lin, Phys. Rev. B **30**, 1448 (1984).
[82] B. Dunweg and K. Binder, Phys. Rev. B **36**, 6935 (1987).
[83] A. Bieber and F. Gautier, J. Magn. Magn. Mater. **99**, 293 (1991).
[84] J. M. Sanchez, J. L. Moran-Lopez, C. Leroux, and M. C. Cadeville, J. Phys. C **21**, L1091 (1988).
[85] A. V. Ruban and H. L. Skriver, Phys. Rev. B **55**, 856 (1997).
[86] A. Liechtenstein, M. I. Katsnelson, and V. A. Gubanov, J. Phys. F: Met. Phys. **14**, L125 (1984).
[87] A. Liechtenstein, M. I. Katsnelson, V. P. Antropov, and V. A. Gubanov, J. Magn. Magn. Mater. **67**, 65 (1987).
[88] T. Oguchi, K. Terakura, and H. Hamada, J. Phys. F: Met. Phys. **13**, 145 (1983); T. Oguchi, K. Terakura, and A. R. Williams, Phys. Rev. B **28**, 6443 (1983).
[89] N. M. Rosengaard and B. Johansson, Phys. Rev. B **55**, 14 975 (1997).
[90] S. V. Halilov, H. Eschrig, A. Y. Perlov, and P. M. Oppeneer, Phys. Rev. B **58**, 293 (1998).
[91] Y. M. Zhou, D. S. Wang, and Y. Kawazoe, Phys. Rev. B **59**, 8387 (1999).
[92] S. Moran, C. Ederer, and M. Fahnle, Phys. Rev. B **67**, 012407 (2003).
[93] M. Uhl and J. Kubler, Phys. Rev. Lett. **77**, 334 (1996).
[94] M. V. You, V. Heine, A. J. Holden, and P. J. Lin-Chung, Phys. Rev. Lett. **44**, 1282 (1980).
[95] P. Bruno, Phys. Rev. Lett. **90**, 087205 (2003).
[96] J. Staunton, B. L. Györffy, G. M. Stocks, and J. Wadsworth, J. Phys. F: Met. Phys. **16**, 1761 (1986).
[97] J. B. Staunton and B. L. Györffy, Phys. Rev. Lett. **69**, 371 (1992).
[98] M. Pajda, J. Kudrnovsky, I. Turek, V. Drchal, and P. Bruno, Phys. Rev. B **64**, 174402 (2001).
[99] For Heisenberg MC simulations we have used a $20\times20\times20$ box of the bcc underlying lattice. All the pair exchange parameters stronger than 0.01 meV have been included in the Hamiltonian (12 altogether).
[100] V. P. Antropov, S. V. Tretyakov, and B. Harmon, J. Appl. Phys. **81**, 3961 (1997).
[101] V. P. Antropov, J. Magn. Magn. Mater. **262**, L192 (2003).
[102] O. N. Mraysov, A. J. Freeman, and A. I. Lichtenstein, J. Appl. Phys. **79**, 4805 (1996).
[103] V. P. Antropov, M. van Schifgaarde, and B. N. Harmon, J. Magn. Magn. Mater. **140–144**, 1355 (1995).
[104] J. A. Blanco and V. M. Prida Pidal, Eur. J. Phys. **16**, 195 (1995).